Theory of Quantum Transport in Nano and Molecular Scale Systems

Noorah Abdullah Alwhaibi

Ph.D. Thesis in Physics

This thesis is submitted in partial fulfilment of the requirements for the degree of Doctor of Philosophy

2021

Lancaster University

Declaration

Except where stated otherwise, this thesis is a result of the author's original work and has not been submitted in whole or in part for the award of a higher degree elsewhere. This thesis documents work carried out between October 2017 and March 2021 at Lancaster University, UK, under the supervision of Prof. Colin J. Lambert and Dr. Iain M. Grace funded by Qassim University, Saudi Arabia.

Noorah Alwhaibi

To my gorgeous sister Khdijah

To the most beautiful gift I have ever had my son Ibrahim

for their love, endless support, and sacrifices.

Acknowledgements

I would like to express sincere gratitude to my supervisor, Professor Colin J. Lambert, who guided me during my study. His kindness, patience and support are prodigious. I am so appreciative to have worked with such a great physicist. I would also like to express my grateful admiration to Dr Iain Grace ; none of this work would have been accomplished without his insightful comments and suggestions, dedicated time, and guidance.

Also, I would like to extend my thanks to all the co-supervisors, my best friends and all the members of Colin's group who helped me learn something and added a positive impact during my studies. My thanks also go out to the support I received during my PhD from the higher education ministry in Saudi Arabia and Qassim University.

Finally, I am deeply grateful to my parents and my brothers for all of the love, support, encouragement, and prayers they have sent my way along this journey. A massive thank you for Your unconditional love and support has meant the world to me; I hope that I have made you proud.

Abstract

This thesis investigates the fundamental aspects of the molecular-scale junctions and their electrical properties. Experimental and theoretical studies assessed the importance of finding ways to get consistent and reproducible improvements in electronics devices fabrications techniques. In this context, I will start this thesis by introducing a general discussion about using the density functional theory (DFT), and Green's function to study transport calculations at a molecular scale. Then, I will present the theoretical and experimental benzo-(bis)imiadzol molecular studies in chapter 4. This study focusses on changes in the conductance as a consequence of chemical stimuli. I will demonstrate that benzo-bis(imidazole) conductance switching upon protonation depends on the lateral functional groups. The protonated H-substituted molecule shows a higher conductance than the neutral one ($G_{pro}>G_{neu}$), while the opposite ($G_{neu}>G_{pro}$) is observed for a molecule functionalized by amino-phenyl groups. Based on theoretical calculations, I conclude that these opposite behaviours depend on the electronic coupling between molecules and electrodes. Furthermore, quantum interference properties have recently attracted excessive interest in electron transport studies at the single-molecule scale. Within this framework, myself and collaborators have aimed to improve the efficiency of pi-stacked molecules in controlling quantum interference by carefully designing them. Chapter 5 introduces a novel strategy for designing folded carbazoles with low conductance in different structures. This strategy highlights the presence or absence of destructive quantum interference in different configurations. This project is part of a collaborations with the experimental group at the University of Madrid, which is ongoing at present.

List of publications

1. Audi, Hassib, Yannick Viero, **<u>Noorah Alwhaibi</u>**, Zhongrui Chen, Maksym Iazykov, Arnaud Heynderickx, Fan Xiao et al. "Electrical molecular switch addressed by chemical stimuli." *Nanoscale* 12, no. 18 (2020): 10127-10139.

Contents

Chapter 1

Introduction

1.1. Molecular electronics

In recent decades, designing and fabricating nano-scale electronic devices has attracted a wide range of scientific and industrial attention as exploring their unique properties can open up broad miniaturisation revolution prospects [1]. Historically, in 1965, Gordon Moore noted that the number of transistors per unit area or (per chip) in practical applications doubles every two years, that developed into what is known as 'Moore's law' [2]. He expected this trend to continue for ten years, but it lasted a half-century later due to the rapid development in miniaturization. As electronic components approach the sub-10nm length scale, the limit of Moore's law is being reached [2]. Therefore, scientists are keen to find an alternative to silicon-based devices by replacing the traditional semiconductor; one such option is a single molecule. Aviram and Ratner have been thought of as critical in the historical of development molecular

devices because they were the first to suggest using an individual molecule as a functional electronic component. In 1974, they proposed the first molecular rectifier where the rectifier is an electrical device that converts alternating current (AC) to direct current (DC), which flows in only one direction. They considered using a single molecule consisting of an electron donor unit (TTF), which is electron rich, and an acceptor unit (TCNE), which is electron poor, separated by tunneling bridge(methylene), and noted that this molecular system functions as a rectifier (one-way conductor) of electric current [3-4]. Later in the 1980s the invention of scanning tunneling microscope (STM) and atomic force microscope (AFM) led to further developments of this field. Another research motivated by Aviram direction was in 1995, where Joachim and Gimzewski [4] published the first measurement of a single-molecule conductance by using the STM technique. In 1997, Mark Reed and James Tour published a first transport experiment results in single-molecule junctions using a mechanically controlled break junction method (MCBJ) method. They connected two gold electrodes to a sulphur-terminated molecular-wire, which realised a symmetric structure that could, in principle, be integrated into more complex circuits [6].

Nowadays, the field of molecular electronics has been advancing rapidly both experimentally and theoretically, using on single-molecule junctions based on metal-molecule-metal designs. In order to study such systems experimentally, many techniques have been developed, such as Scanning Tunneling Microscopy Break Junctions (STM-BJ) [7,8], and Mechanically Controllable Break Junctions MCBJ [9,10]. The development of theoretical approaches in line with experiment, provide reliable and excellent methods for calculating the electronic assembly of atomic structures. One of the most widely used approach is Density Functional Theory (DFT) based quantum transport calculations which is the method used for the calculations in

this thesis. One widely used DFT code is SIESTA [11], enabling the study of finite and periodic systems [12-13].

Moreover, combining DFT with the Green's function formalism allows one to study molecular structures connected to bulk electrodes [14]. One implementation of this is the Gollum code[15], which will be used extensively within this thesis. Associating experimental data with a validated theoretical framework paved the way for understanding electron transport properties in these molecular junctions. This combination of theory and experiment enables the exploration of new devices, with the aim of optimizing both the electrical and thermal transport behaviour through chemical design. One area where this has proved successful has been the investigation of room-temperature quantum interference [16].

1.2. Molecular Junctions

Molecular junctions are the ideal systems to get insight into the fundamental electron transport mechanism. In a two terminal system they consist of left and right electrodes, the linkers (or anchor groups) and the central molecule, as shown in Figure (1.1). The choice of anchor groups, which bind the molecule to the electrode surface is important as they are determined by the type of electron transport (ie HOMO or LUMO dominated). Furthermore, electrodes can be either metal or nonmetal, for example silicon has been used as an electrode [17] However, metallic materials are the most widely used with examples such as Au, Ag [18]and Pt [19] being reported. Gold is the most common material used, because it is inert to chemical reactions, has good chemical stability, high conductivity, and is easy to prepare in the form of clean surfaces and tips. However, gold electrodes also have several drawbacks, such as mobility of

surface atoms at room temperature, which cause thermal fluctuations and instabilities [6].
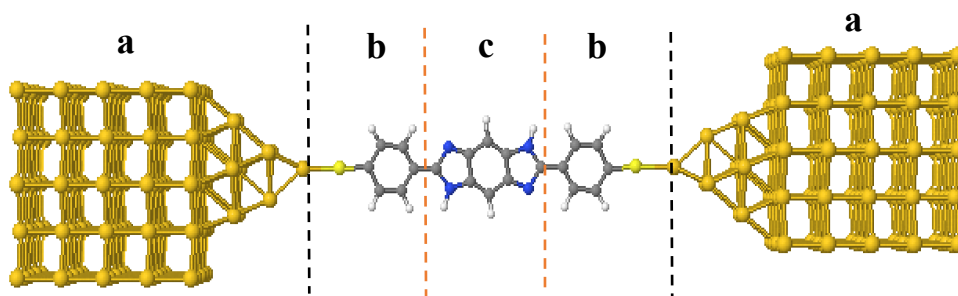

Figure 1.1. Schematic illustration of molecular junction consists of (a)left and right gold electrodes (b) The linker which is here thiol as anchor groups and Benzene rings at the both sides of the central area.(c) central molecule as an example Benzo(bis)imidazole.

In this respect, it is essential that research of other materials, which will ultimately affect the implementation in molecular electronics devices. In recent years, the possibility of making reliable single molecule electrical measurements with other non-metallic electrodes such as carbon-based materials, and graphene has been investigated[20,21]. Their unique advantages make them promising molecules because of their electronic properties with high stability and chemical flexibility due to their π-conjugated structure. Many types of molecular junctions have been studied with gold electrodes, which has included different anchoring groups and linkers. The anchor assembly is a single point contacts chemically bind to metallic leads, for example, thiol (-SH), amine (-NH2) groups, where the linker is a reliable contact linked with anchor unit between the central molecule and the gold electrodes, such as a phenyl ring and porphyrin[16].

Another fundamental ingredient in the design of molecular junction devices is the molecule conformation, which is fascinating since there is an almost infinite variety of configurations to consider for molecular electronics. Using molecules as electronic circuits in nano-scale devices are highly desirable, because of their small sizes typically only a few nanometers, and the low cost of producing large numbers of identical molecules. Their ability to be self-assemble onto surfaces, allows the molecular units to naturally form themselves into ordered structures by non-covalent interactions. Moreover, a molecular wire could reduce the transit time ($\sim10^{-14}$ S) needed for an operation[6]. Here, the focus is on *Conjugated* or '*Aromatic*' *Hydrocarbon* compounds, which are generally compounds containing at least one ring consisting of six carbon atoms, such as Benzene and Anthracene, where each carbon atom is joined by alternating of double and single bonds, and the wave functions of the π system is delocalised over the whole molecule. However, it is not essential to have simply a benzene ring to be an aromatic molecule, as there are various molecules containing heteroatoms (O,N,S) that are also aromatic, for instance, pyridine[6]. Furthermore, molecules consisting of several benzene rings are called '*polycyclic aromatic Hydrocarbons*', such as, Benzo-imidazole and carbazole, as are discussed in the next section. Notable applications of electronic devices using single molecules in various fields, include such as transistors[22], rectifiers[23, 24], sensors[25,26], and memories [27]. However, it is essential to have recognition of an individual molecule's properties to fabricate molecular devices, as the ability to use a specific intermolecular interaction to assemble these devices correctly and control the electron transport between the molecule and electrodes has remained challenging due to molecule size, and instabilities at high temperature[6] [28].

1.2.1. Structure of Benzo-imidazole

In chapter 4 I study molecular junctions formed from Benzo-imidazole molecules, which are heterocyclic aromatic organic compounds, formed from the fusion of benzene and imidazole. When two imidazoles are fused on the side of the Benzene ring, the resulting molecule is called Benzo-bis(imidazole) and is shown in figure(1.2)(a, b) respectively. The term 'heterocyclic' refers to multiple rings with one or more carbon atoms are substituted by another species of atom.
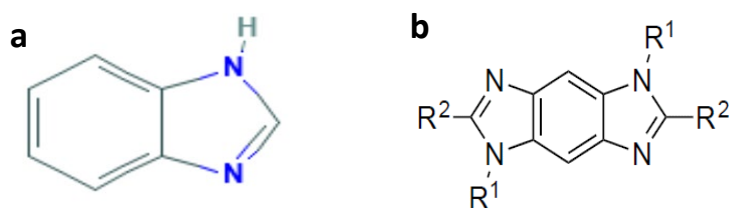
Figure 1.2. General structure of(a) Benzo-imidazole, (b) Benzo-bis(imidazole).

1.2.2. Structure of carbazole

In chapter 5 I investigate pi-stacking using carbazole molecules. Carbazole is an aromatic organic compound. It has a tricyclic structure, consisting of two six-membered benzene rings fused on either side of a five-membered nitrogen-containing ring, as shown in Figure(1.3). Later I will utilise the carbazole unit within molecular cores to investigate an alternative method to control quantum interference in the pi-stacked system.

Figure 1.3. Carbazole chemical structure in(a) 2D, (b)3D.

1.3. Quantum interference

In recent years, studies of charge transport at the molecular- scale, have led to significant interest in quantum interference (QI) effects [29-32], which provide a novel opportunity to tune and control transport via the electron wave function within a junction. These effects can enhance or decrease conductance via. constructive or destructive quantum interference respectively. [33]. Since 1988, researchers hav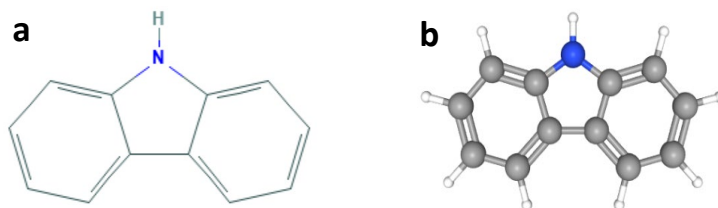e been utilising and exploring the quantum interference (QI) concept theoretically and experimentally, they used the simple structures to study the QI, which is a benzene ring with meta connectivity, and it has been suggested that different paths through molecule might be responsible for the low conductivity as it is assigned to destructive quantum interference (DQI). Manipulating QI provides a potential opportunity to construct molecular electronic devices based on this feature by chemical modifications (explained in detail at chapter 4) or the use of more complex structures. Our focus in chapter five will be on one of these effects, namely destructive quantum interference (DQI) in pi-stacked molecules junctions. DQI describes a quantum process in which the electron waves propagate and then combine destructively at the source or drain electrode [31,34]. This phenomenon greatly influences the electron transmission, and therefore the molecular conductance, which reduces the transmission probability by orders of magnitude compared with junctions exhibiting constructive interference (CQI) [31,35]. Such effects can be used to design single-molecule electronic components, thermoelectric devices [36-37], and molecular switches[29]. Several studies have investigated forms of molecules that show DQI, such as conjugated molecules, and molecules with pendant groups. It is interesting to note that the DQI mostly depends on the molecule's electronic configurations and where the electrodes

contact the molecule [38-39]. One of the conjugated structures shows excellent potential in controlling quantum interference by stacking molecules [34,40] where the electrodes are attached to one anchor at the end of each dimer. Moreover, this will bridge the gap between the electrodes and the electron path between them via the overlap π -orbitals of the molecules. Understanding charge transfer through π-stacked assemblies and controlling DQI, plays an essential role in designing and developing high-performance molecular devices.

1.4. Thesis Outline

This thesis begins with a review of the theoretical techniques used to study electron transport in molecular-scale junctions. The main theoretical approaches based on Density Functional Theory (DFT), and the non-equilibrium Greens function formalism of transport theory are explained in chapters 2 and 3 respectively. These chapters will provide the fundamental theoretical background for understanding and analysing the electrical conductance and its properties in the structures discussed in chapters 4 and 5. Chapter 4 describes a theoretical and experimental study aimed at demonstrating conductance switching in benzo-bis(imidazole) molecule and its derivatives. In the fifth chapter, I will investigate how to control quantum interference in different π-stacked Carbazole molecular junctions using SIESTA and GOLLUM. Finally, the sixth chapter presents the suggestions for future works and conclusion.

Bibliography

[1] Kiguchi, M. (2016). Single-Molecule Electronics. Singapore: Springer.

[2] Moore, G. E. (2009). Cramming more components onto integrated circuits, Reprinted from Electronics, volume 38, number 8, April 19, 1965, pp.114 ff. *IEEE Solid-State Circuits Society Newsletter*, *11*(3), 33–35. https://doi.org/10.1109/n-ssc.2006.4785860

[3] Kasap, S. (2006). *Springer handbook of electronic and photonic materials*. Springer Science & Business Media.

[4] Aviram, A. and Ratner, M. A. (1974). Molecular rectifiers. *Chemical Physics Letters*, *29*(2), 277–283. https://doi.org/10.1016/0009-2614(74)85031-1

[5] Joachim, C., Gimzewski, J. K., Schlittler, R. R. and Chavy, C. (1995). Electronic transparence of a single C 60 molecule. *Physical review letters*, *74*(11), 2102.

[6] Scheer, E. and Cuevas, J. C. (2017). *Molecular electronics: an introduction to theory and experiment* (Vol. 15). World Scientific.

[7] Li, C., Pobelov, I., Wandlowski, T., Bagrets, A., Arnold, A., & Evers, F. (2008). Charge transport in single Au | alkanedithiol | Au junctions: Coordination geometries and conformational degrees of freedom. *Journal of the American Chemical Society*, *130*(1), 318–326. https://doi.org/10.1021/ja0762386

[8] Manrique, D. Z., Huang, C., Baghernejad, M., Zhao, X., Al-Owaedi, O. A., Sadeghi, H., Kaliginedi, V., Hong, W., Gulcur, M., Wandlowski, T. and Bryce, M.R. and Lambert, C. J. (2015). A quantum circuit rule for interference effects in single-molecule electrical junctions. *Nature communications*, *6*(1), 1-8.

[9] Teresa González, M., Wu, S., Huber, R., Van Der Molen, S. J., Schönenberger, C. and Calame, M. (2006). Electrical conductance of molecular junctions by a robust statistical analysis. *Nano Letters*, *6*(10), 2238–2242. https://doi.org/10.1021/nl061581e

[10] Reed, M. A., Zhou, C., Muller, C. J., Burgin, T. P. and Tour, J. M. (1997). Conductance of a molecular junction. *Science*, *278*(5336), 252–254. https://doi.org/10.1126/science.278.5336.252

[11] Soler, J. M., Artacho, E., Gale, J. D., García, A., Junquera, J., Ordejón, P. and Sánchez-Portal, D. (2002). The SIESTA method for ab initio order-N materials simulation. *Journal of Physics Condensed Matter*, *14*(11), 2745–2779. https://doi.org/10.1088/0953-8984/14/11/302

[12] Thoss, M. and Evers, F. (2018). Perspective: Theory of quantum transport in molecular junctions. *Journal of Chemical Physics*, *148*(3). https://doi.org/10.1063/1.5003306

[13] Xue, Y. and Ratner, M. A. (2005). Theoretical principles of single-molecule electronics: A chemical and mesoscopic view. *International Journal of Quantum Chemistry*, *102*(5 SPEC. ISS.), 911–924. https://doi.org/10.1002/qua.20484

[14] Payne, M. C., Teter, M. P., Allan, D. C., Arias, T. A. and Joannopoulos, J. D. (1992). Iterative minimisation techniques for ab initio total-energy calculations: Molecular dynamics and conjugate gradients. *Reviews of Modern Physics*, *64*(4), 1045–1097. https://doi.org/10.1103/RevModPhys.64.1045

[15] Ratner, M. (2013). A brief history of molecular electronics. *Nature nanotechnology*, *8*(6), 378-381.

[16] Lambert, C. J. (2015). Basic concepts of quantum interference and electron transport in single-molecule electronics. *Chemical Society Reviews*, *44*(4), 875–888. https://doi.org/10.1039/c4cs00203b

[17] Ashwell, G. J., Phillips, L. J., Robinson, B. J., Urasinska-Wojcik, B., Lambert, C. J., Grace, I. M., Bryce, M.R., Jitchati, R., Tavasli, M., Cox, T.I. and Sage, I.C. (2010). Molecular bridging of silicon nanogaps. *ACS nano*, *4*(12), 7401-7406.

[18] Kim, T., Vázquez, H., Hybertsen, M. S. andVenkataraman, L. (2013). Conductance of molecular junctions formed with silver electrodes. *Nano letters*, *13*(7), 3358-3364.

[19]. García-Suárez, V. M., Rocha, A. R., Bailey, S. W., Lambert, C. J., Sanvito, S. and Ferrer, J. (2005). Single-channel conductance of H 2 molecules attached to platinum or palladium electrodes. Physical Review B, 72(4), 045437.

[20] Zheng, X. H., Zhang, G. R., Zeng, Z., García-Suárez, V. M., & Lambert, C. J. (2009). Effects of antidots on the transport properties of graphene nanoribbons. *Physical review b*, *80*(7), 075413.

[21] Finch, C. M., Sirichantaropass, S., Bailey, S. W., Grace, I. M., Garcia-Suarez, V. M. and Lambert, C. J. (2007). Conformation dependence of molecular conductance: chemistry versus geometry. *Journal of Physics: Condensed Matter*, *20*(2), 022203.

[22] Perrin, M. L., Burzurí, E. and Van Der Zant, H. S. J. (2015). Single-molecule transistors. *Chemical Society Reviews*, *44*(4), 902–919. https://doi.org/10.1039/c4cs00231h

[23] Batra, A., Darancet, P., Chen, Q., Meisner, J. S., Widawsky, J. R., Neaton, J. B., and Venkataraman, L. (2013). Tuning rectification in single-molecular diodes. *Nano Letters*, *13*(12), 6233–6237. https://doi.org/10.1021/nl403698m

[24] Zhao, J., Zeng, C., Cheng, X., Wang, K., Wang, G., Yang, J., Hou, J.G. and Zhu, Q. (2005). Single C59N molecule as a molecular rectifier. *Physical Review Letters*, *95*(4), 1–4. https://doi.org/10.1103/PhysRevLett.95.045502

[25] Sadeghi, H., Algaragholy, L., Pope, T., Bailey, S., Visontai, D., Manrique, D., Ferrer, J., Garcia-Suarez, V., Sangtarash, S. and Lambert, C.J. (2014). Graphene sculpturene nanopores for DNA nucleobase sensing. *Journal of Physical Chemistry B*, *118*(24), 6908–6914. https://doi.org/10.1021/jp5034917

[26] Sadeghi, H., Bailey, S. andLambert, C. J. (2014). Silicene-based DNA nucleobase sensing. *Applied Physics Letters*, *104*(10). https://doi.org/10.1063/1.4868123

[27] Prodromakis, T., Toumazou, C. and Chua, L. (2012). Two centuries of memristors. *Nature Materials*, *11*(6), 478–481. https://doi.org/10.1038/nmat3338

[28] Pijper, T. C., Kudernac, T., Katsonis, N., van der Maas, M., Feringa, B. L. and van Wees, B. J. (2013). Reversible light induced conductance switching of asymmetric diarylethenes on gold: surface and electronic studies. *Nano-scale*, *5*(19), 9277-9282.

[29] Baer, R. and Neuhauser, D. (2002). Phase coherent electronics: A molecular switch based on quantum interference. *Journal of the American Chemical Society*, *124*(16), 4200–4201. https://doi.org/10.1021/ja016605s

[30] Cardamone, D. M., Stafford, C. A. and Mazumdar, S. (2006). Controlling quantum transport through a single molecule. *Nano Letters*, *6*(11), 2422–2426. https://doi.org/10.1021/nl0608442

[31] Guédon, C. M., Valkenier, H., Markussen, T., Thygesen, K. S., Hummelen, J. C. and Van Der Molen, S. J. (2012). Observation of quantum interference in molecular charge transport. *Nature Nanotechnology*, *7*(5), 305–309. https://doi.org/10.1038/nnano.2012.37

[32] Lambert, C. J. (2021). Quantum Transport in Nanostructures and Molecules.

[33] Liu, J., Huang, X., Wang, F. and Hong, W. (2019). Quantum Interference Effects in Charge Transport through Single-Molecule Junctions: Detection, Manipulation, and Application. *Accounts of Chemical Research*, *52*(1), 151–160. https://doi.org/10.1021/acs.accounts.8b00429

[34] Frisenda, R., Janssen, V. A. E. C., Grozema, F. C., Van Der Zant, H. S. J. and Renaud, N. (2016). Mechanically controlled quantum interference in individual Ï-stacked dimers. *Nature Chemistry*, *8*(12), 1099–1104. https://doi.org/10.1038/nchem.2588

[35] Garner, M. H., Li, H., Chen, Y., Su, T. A., Shangguan, Z., Paley, D. W., Liu, T., Ng, F., Li, H., Xiao, S. and Nuckolls, C. (2018). Comprehensive suppression of single-molecule conductance using destructive σ-interference. *Nature*, *558*(7710), 415-419.

[36] Kiršanskas, G., Li, Q., Flensberg, K., Solomon, G. C. and Leijnse, M. (2014). Designing π-stacked molecular structures to control heat transport through molecular junctions. *Applied Physics Letters*, *105*(23). https://doi.org/10.1063/1.4903340

[37] Li, Q. and Solomon, G. C. (2014). Exploring coherent transport through π-stacked systems for molecular electronic devices. *Faraday Discussions*, *174*, 21–35. https://doi.org/10.1039/c4fd00083h

[38] Reuter, M. G. and Hansen, T. (2014). Communication: Finding destructive interference features in molecular transport junctions.

[39] Liu, X., Sangtarash, S., Reber, D., Zhang, D., Sadeghi, H., Shi, J., Xiao, Z.Y., Hong, W., Lambert, C.J. and Liu, S.X.(2017). Gating of quantum interference in molecular junctions by heteroatom substitution. Angewandte Chemie, 129(1), 179-182.

[40] Martín, S., Grace, I., Bryce, M. R., Wang, C., Jitchati, R., Batsanov, A. S. and Nichols, R. J. (2010). Identifying diversity in nano-scale electrical break junctions. *Journal of the American Chemical Society*, *132*(26), 9157–9164. https://doi.org/10.1021/ja103327f

Chapter 2

Density Functional Theory

2.1. Introduction

Understanding the electronic properties of an isolated molecular wire can help to explain and investigate the behaviour of molecular electronics devices, which is the focus of this thesis. In an attempt to solve the interacting many-body Schrödinger equation and determine the structural and electronic behaviour of organic molecules, a reliable methodology is necessary. Density function theory (DFT) is one of the essential theoretical tools used by physicists and chemist to achieve more understanding in the electronic structure[2][3][4][5][6][7][8]. This theory incorporates the Kohn-Sham formalism, which is the one-electron Schrödinger equation of a fictitious system (the

"Kohn–Sham system") of non-interacting particles (typically electrons) that generate the same density as any given system of interacting particles. [3][4]

In this chapter, I will present the main details of DFT and introduce the DFT code 'SIESTA' (*S*panish *I*nitiative for *E*lectronic *S*imulations with *T*housands of *A*toms) [1], which I have used widely during my PhD studies as a theoretical tool to study the configurations of molecules as well as calculating charge densities, band structures, and binding energies.

The first section will be an introduction to DFT, outlining the prominent formalism as a method of solving the many-particle time-independent Schrödinger equation. Then, presenting the physical theories that have significant development to turn DFT to a data processing code (SIESTA)[1] which are the Hohenberg-Kohn Theorem and the Kohn-Sham Formulation.

The second section, emphasising the application of DFT, via SIESTA, and how I can employ these techniques to reduce the complexity of the problem and perform reliable, accurate calculations on molecular structures despite how large scale these systems.

2.2. The Schrödinger Equation

Finding the solution of the Schrödinger equation is only possible for a few number of electrons. However, for larger systems, solving the many-body Schrödinger equations is challenging, insoluble and has been a goal for physicists and chemists to achieve. In general, the Hamiltonian of the many-body system consisting of N interacting electrons and M nucleons is divided into five parts and can be written as:

$$\hat{H} = \hat{T_e} + \hat{T_n} + \hat{V_n} + \hat{V_e} + \hat{V_{en}} \tag{2.1}$$

Where,

$$\hat{H} = -\overbrace{\frac{\hbar^2}{2m_e}\sum_{i=1}^{N}\nabla_i^2}^{\hat{T_e}} - \overbrace{\frac{\hbar^2}{2m_n}\sum_{n=1}^{M}\nabla_n^2}^{\hat{T_n}} + \overbrace{\frac{1}{4\pi\varepsilon_o}\frac{1}{2}\sum_{n=1}^{M}\sum_{n\neq n'}^{M}\frac{1}{|\vec{R}_n-\vec{R}_{n'}|}Z_nZ_{n'}e^2}^{\hat{V_n}} +$$

$$\overbrace{\frac{1}{4\pi\varepsilon_o}\frac{1}{2}\sum_{i=1}^{N}\sum_{i\neq j}^{N}\frac{e^2}{|\vec{r}_i-\vec{r}_j|}}^{\hat{V_e}} + \overbrace{\frac{1}{4\pi\varepsilon_o}\frac{1}{2}\sum_{i=1}^{N}\sum_{n=1}^{M}\frac{1}{|\vec{r}_i-\vec{R}_n|}Z_ne^2}^{\hat{V_{en}}} \tag{2.2}$$

where $\hat{T_e}$ is the kinetic energy of the electron, $\hat{T_n}$ is the kinetic energy of nuclei, $\hat{V_n}$ is the nucleon-nucleon interaction, $\hat{V_e}$ is the electron-electron interaction , $\hat{V_{en}}$ is the electron nucleon interaction, Z is the atomic number ,and e is the electron charge Solving the Schrödinger equation for a simple system such as the Hydrogen atom is obtainable in order to get the wave function of this system. It is impossible to find the exact solution of the Schrödinger equation for the many-body system with more than a few electrons. An approximation has to be therefore applied to enable a separation of the nucleon and electron degrees of freedom to reduce the size of the problem. This is achieved through the Born-Oppenheimer approximation. [9]

2.3. Born-Oppenheimer approximation

We can simplify the equation by using the Born-Oppenheimer approximation, which due to the fact that the mass of the nuclei is much larger than the electron (at least three orders of magnitude larger) [9][10] allows the nuclei to be considered fixed

and therefore their kinetic energy is zero. [9]. Thus, the Hamiltonian reduces to the new electronic Hamiltonian $\widehat{H}_e$, defined as follows.

$$\hat{H}_e = \sum_{i=1}^{N} \frac{-\hbar^2}{2m_i} \nabla_i^2 + \frac{1}{4\pi\varepsilon_o} \frac{1}{2} \sum_{i \neq j}^{N} \frac{e^2}{|r_i - r_j|} + \frac{1}{4\pi\varepsilon_o} \frac{1}{2} \sum_{in}^{NM} \frac{Z_n e^2}{|r_i - R_n|} \qquad (2.3)$$

And the Nucleon Hamiltonian $\widehat{H_N}$,

$$\widehat{H_N} = \sum_{n}^{M} - \frac{\hbar^2 \nabla_n^2}{2m_n} - \frac{1}{2} \sum_{n \neq n'}^{M} \frac{Z_n Z_{n'} e^2}{4\pi\epsilon_0 |R_n - R_{n'}|} \qquad (2.4)$$

Therefore, the Born-Oppenheimer approximation allows the electron and nucleon degrees of freedom to be separated. The general method in solving the system of electrons and nucleons is to first solve the effective electron Hamiltonian using DFT, Hartree, Hartree-Fock or other quantum mechanical methods, and then treat the nucleon equations as classical equations of motion. The majority of the chapter will be devoted to methods in solving the effective electron Hamiltonian $\widehat{H_e}$.

2.4. The Hohenberg-Kohn theorems

The essential building blocks of Density Functional Theory, which mainly describe the method of solving the Schrödinger equation defined by $\widehat{H_e}$, is based on two crucial theories in the pioneering work of Hohenberg and Kohn in 1964 [5]. These show that there is a unique ground state density of the system which corresponds to a minimum of the total energy functional. The electron density ρ (r) is used to calculate the ground state energy and can be applied to any system of electrons moving in an external potential.

The first theorem of this approximation states that the ground state electronic density is uniquely determined by only one external potential which means that there cannot be two external potentials where $V_{ext2}(\vec{r}) \neq V_{ext1}(\vec{r}) + constant$ leading to same ground state density. If we assume that there are two Hamiltonian and different external potentials where $V_{ext2}(\vec{r}) \neq V_{ext1}(\vec{r}) + constant$ cannot give rise to same ground state density $\rho_{GS}(\vec{r})$[5,7,8,12].

Proof (1): this theorem can be proven via a contradiction . Let us consider two different external potentials $V_{ext}(\vec{r})_{(1)}$ and $V_{ext}(\vec{r})_{(2)}$ which differ by more than a constant and yield the same ground state density $\rho_{GS}(\vec{r})$. Clearly, these potentials correspond to distinct Hamiltonians which are $H_{ext}[(\vec{r})]_{(1)}$ and $H_{ext}[(\vec{r})]_{(2)}$, these Hamiltonians give rise to distinct wavefunctions which are $\Psi_{ext}[(\vec{r})]_{(1)}$ and $\Psi_{ext}[(\vec{r})]_{(2)}$.

Since we have the same ground state and according to the variational principle which states that no wavefunction gives energy less than the energy of $\Psi_{ext}[(\vec{r})]_{(1)}$ for $H_{ext}[(\vec{r})]_{(1)}$, i.e.,

$$\langle E_{(1)} \rangle = \int \Psi_{(1)} H_{(1)} \Psi_{(1)}^* \, d\vec{r} < \int \Psi_{(2)} H_{(2)} \Psi_{(2)}^* \, d\vec{r} \qquad (2.5)$$

Because of the same ground state densities for two Hamiltonians, the equation (2.5) for non-degenerate ground state becomes:

$$\int \Psi_{(2)} H_{(1)} \Psi^*_{(2)} \, d\vec{r}$$

$$= \overbrace{\int \Psi_{(2)} H_{(2)} \Psi^*_{(2)} \, d\vec{r}}^{\langle E_{(2)} \rangle} \tag{2.6}$$

$$+ \int \left\{ [V_{ext}(\vec{r})]_{(1)} - [V_{ext}(\vec{r})]_{(2)} \right\} \rho_{GS}(\vec{r}) \, d\vec{r}$$

By exchanging the labels in equation (2.6), we have:

$$\int \Psi_{(1)} H_{(2)} \Psi^*_{(1)} \, d\vec{r} =$$

$$= \overbrace{\int \Psi_{(1)} H_{(1)} \Psi^*_{(1)} \, d\vec{r}}^{\langle E_{(1)} \rangle} \tag{2.7}$$

$$+ \int \left\{ [V_{ext}(\vec{r})]_{(2)} - [V_{ext}(\vec{r})]_{(1)} \right\} \rho_{GS}(\vec{r}) \, d\vec{r}$$

Adding the equations (2.6) and (2.7) we obtain:

$$\langle E_{(1)} \rangle + \langle E_{(2)} \rangle < \langle E_{(2)} \rangle + \langle E_{(1)} \rangle \tag{2.8}$$

Equation (2.8) evidently shows a contradiction. Therefore we can conclude that the potential $V_{ext}(r)$, must be unique.

Theorem (2) provides a variational ansatz for obtaining $\rho(\vec{r})$, i.e., searching for $\rho(\vec{r})$ which minimises the energy. In other words, it states that we can define a universal functional for the energy $E[\rho(\vec{r})]$ in terms of the density, $\rho(\vec{r})$. The exact ground state energy of the system in particular ($V_{ext}(\vec{r})$) is the global minimum value of this functional and the density, $\rho(\vec{r})$, which minimizes the functional and represents the exact ground state density, $\rho_{GS}(\vec{r})$ [5,7,8,12].

Proof (2), the first theorem tells us that the total energy of the system is a functional of the density, $\rho(\vec{r})$, and is given by

$$E_{total}[\rho(\vec{r})]$$

$$= T_{int}[\rho(\vec{r})] + \overbrace{\underbrace{V_e[\rho(\vec{r})]}_{\substack{=zero,\ for \\ non-interacting \\ system}}}^{F_{H-K}[\rho(\vec{r})]} + \int V_{ext}(\vec{r})\ \rho(\vec{r})\ d\vec{r} \qquad (2.9)$$

The first two terms in equation (2.9) ($F_{H-K}[\rho(\vec{r})]$) are the kinetic energy for interaction system (T_{int}), and the electron-electron interaction energy (V_e), is treated as the same for the whole system. Thus $F_{H-K}[\rho(\vec{r})]$ is a universal functional. Assuming that the system is in the ground state, we can define the energy uniquely by the ground state density, $\rho_{GS}(\vec{r})$, as:

$$\langle E_{GS} \rangle = \langle E[\rho_{GS}(\vec{r})] \rangle = \int \Psi_{GS}\ H_{GS}\ \Psi_{GS}^*\ d\vec{r} \qquad (2.10)$$

According to the variational principle, the ground state energy corresponds to the ground state density is the minimum energy, and any different density will necessarily provide higher energy

$$\langle E_{GS} \rangle = \langle E[\rho_{GS}(\vec{r})] \rangle = \int \Psi_{GS}\ H_{GS}\ \Psi_{GS}^*\ d\vec{r} < \int \Psi\ H\ \Psi^*\ d\vec{r}$$

$$\qquad (2.11)$$

$$= \langle E[\rho(\vec{r})] \rangle\ \ = \langle E \rangle$$

Once we know the functional, $F_{H-K}[\rho(\vec{r})]$, we can minimize the total energy with respect to variations in the density function as given in equation (2.9), that leads to determining the exact ground state properties of the system that we are looking for (we should take into account that for the most practical calculations, the direct minimization will not provide us the ground state energy, but by the simpler procedure of Kohn-Sham).

2.5. The Kohn-Sham Approach

The Kohn–Sham equation [4] is the Schrödinger equation of a fictitious system of non- interacting particles, which generate the same density as any given system of interacting particles (a self-consistent method) [2,4]. Kohn and Sham introduced a solution that it is possible to replace the original Hamiltonian of the system by an effective Hamiltonian (H_{eff}) of the non-interacting system in an effective external potential V_{eff} ($\vec{r}$) which gives rise to the same ground state density as the original system. Since there is no exact recipe for calculating this, the Kohn-Sham method is considered as an ansatz, but it is considerably easier to solve than the non-interacting problem The Kohn-Sham method is based on the Hohenberg-Kohn universal density:

$$F_{H-K}[\rho(\vec{r})] = T_{int}[\rho(\vec{r})] + V_e[\rho(\vec{r})] \qquad (2.12)$$

The Hohenberg-Kohn functional for non-interacting electrons have only the kinetic energy. The energy functional of the Kohn-Sham ansatz $F_{KS}[\rho(\vec{r})]$, in contrast to (2.9), is given by

$$F_{KS}[\rho(\vec{r})] = T_{non}[\rho(\vec{r})] + E_{Hart}[n\rho(\vec{r})] + \int V_{ext}(\vec{r})\,\rho(\vec{r})\,d\vec{r}$$

$$+E_{xc}[\rho(\vec{r})] \qquad (2.13)$$

where T_{non} is the kinetic energy of the non-interacting system which is different from T_{int} (for interaction system) in equation (2.9), while E_{Hart} which is called the Hartree energy is the classical electrostatic energy or classical self-interaction energy of the electron gas which is associated with density $\rho(\vec{r})$. The fourth term, E_{xc}, is the exchange-correlation energy functional which is the difference between the kinetic energy for the interacting and non-interacting systems and non-classical electrostatic interaction energy, and is given by

$$E_{xc}[\rho(\vec{r})] = F_{H-K}[\rho(\vec{r})] - \overbrace{\frac{1}{2}\int \frac{\rho(\vec{r}_1)\rho(\vec{r}_2)}{|\vec{r}_1 - \vec{r}_2|} d\vec{r}_1 d\vec{r}_2}^{E_{Hart}[\rho(\vec{r})]} - T_{non}[\rho(\vec{r})] \qquad (2.14)$$

The first, second, and third terms in the equation (2.13) can be trivially cast into a functional form. In contrast, there is, in general, no exact functional form exist for E_{xc}. In the last couple of decades, enormous efforts have gone into finding a better approximation to E_{xc}. Currently, the functionals can be used to investigate and predict the physical properties of a wide range of solid state systems and molecules. For the

last three terms in the equation (2.13), we take the functional derivatives to construct the effective single particle potential, $V_{eff}(\vec{r})$

$$V_{eff}(\vec{r}) = V_{ext}(\vec{r}) + \frac{\partial E_{Hart}[\rho(\vec{r})]}{\partial \rho(\vec{r})} + \frac{\partial E_{xc}[\rho(\vec{r})]}{\partial \rho(\vec{r})} \qquad (2.15)$$

Now, we can use this potential to give the Hamiltonian of the single particle

$$H_{KS} = T_{non} + V_{eff} \qquad (2.16)$$

By using this Hamiltonian, the Schrödinger equation becomes

$$[T_{non} + V_{eff}]\Psi_{KS} = E\Psi_{KS} \qquad (2.17)$$

Equation (2.17) is known as Kohn-Sham equation. The Kohn-Sham approach shows that a complicated many-body system can be mapped onto a set of simple non-interacting equations exactly if the exchange-correlation functional is known. However, the exchange-correlation functional is not known exactly, so approximations need to be made.

2.5.1 Exchange and correlation

Density functional theory reduces the quantum mechanical ground-state many-body problem to one single body problem, by the Kohn-Sham equations [8]. This method is formally precise, while for practical calculations, the exchange-correlation energy, E_{xc}, as a function of the density has to be approximated. To do that, the local density approximation (LDA) has long been the standard choice [13]. Despite its simple nature, the predictions made using LDA gives realistic descriptions of the atomic structure, elastic, and vibrational characteristics for a wide range of systems. Yet, LDA is generally not accurate enough to describe the energetics of chemical reactions (heats of reaction and activation energy barriers), which lead to an overestimate of the binding energies of molecules and solids. As well, there are numerous examples where the LDA puts molecular conformations or crystal bulk phases in an even qualitatively wrong energetic order [14][15].

Recently, generalised gradient approximations (GGA's) have overcome such deficiencies to a considerable extent [8][16], giving, for example, a more realistic description of energy barriers in the dissociative adsorption of hydrogen on metal and semiconductor surfaces [24]. Gradient corrected (GGA) functional depends on the local density and the spatial variation of the density. So, the two most common functionals used are LDA and GGA to describe the exchange and correlation energies in density functional theory. To give more information about the Local Density Approximation and the Generalised Gradient Approximation, the following section will briefly describe it.

2.5.1.1.Local Density Approximation

The LDA approximation assumes that the exchange-correlation functional depends only on the local density which was introduced by Kohn and Sham [3][4] and it, therefore, can be expected to give good predictions for systems where the density is varying slowly locally. The functional of the approximation is [4]

$$E_{xc}^{LDA}[\rho(\vec{r})] = \int \rho(\vec{r}) E_{xc}^{HGE}[\rho(\vec{r})] \, d(\vec{r}) \tag{2.18}$$

Where E_{HGE}^{xc} is the exchange-correlation energy of the homogeneous electron gas with a density of $(\vec{r})$. The exchange-correlation energy E_{xc}^{HGE} can be split into two terms as the - sum of the exchange $E_x^{HGE}[\rho(\vec{r})]$ and the correlation energies $E_c^{HGE}[\rho(\vec{r})]$ which can be found separately as:

$$E_{xc}^{LDA} = \int d(\vec{r}) \rho(\vec{r}) E_x^{HGE}[\rho(\vec{r})] + E_c^{HGE}[\rho(\vec{r})] \tag{2.19}$$

However, in some sense, the simplest method one can imagine for the exchange and correlation energies is LDA, which can be accurate for the systems with S and P orbitals like graphene and carbon nanotubes or where the electron density is not rapidly changing.

2.5. Generalized gradient approximation

The LDA approximation fails in situations where the density is changing rapidly, such as in molecules. Thus, the LDA method has been extended by involving the

derivatives of the density into the functional method of the exchange-correlation energies. The only way to do this is by including the gradient and the higher spatial derivatives of the total charge density ($|\nabla\rho(\vec{r})|$, $|\nabla^{\wedge 2}\ \rho(\vec{r})|$,...) into the approximation. Such a function is called the generalised gradient approximation (GGA).

$$E_{xc}^{GGA}[\rho(\vec{r})] = \int \rho(\vec{r})\varepsilon_{xc}^{GGA}[\rho(\vec{r}), |\nabla\rho(\vec{r})|]d(\vec{r}) \qquad (2.20)$$

2.6 SIESTA

The implementation of DFT used to obtain the relaxed geometry of the discussed structures, and also to carry out the calculations to investigate their electronic properties. SIESTA (derived from the Spanish Initiative for Electronic Simulations with Thousands of Atoms), is a self-consistent density functional theory technique that uses norm-conserving pseudopotentials, and an Linear Combination of Atomic Orbital Basis set, to perform efficient calculations [1].

To discover more theoretical details about SIESTA code, and what it provides, the next section will describe some of SIESTA's components and how they implemented within the code. [17].

2.5.1 The Pseudopotential Approximation

A pseudopotential or effective potential is another approximation created to solve the many-body Schrödinger equation by reducing the number of electrons involved in

the simulation. This approximation can be achieved by splitting the electrons into two types. The two forms consist of the core electrons in which the electrons occupy the filled shells of the atomic orbitals and the valence electrons which lie in the partially filled shells. By replacing the core electrons, so that they approximate the potential in such a way that the valence electrons felt the core electrons, then a pseudopotential is constructed. It is noted that the core electrons in most molecules do not contribute to the formation of the molecular orbitals.

This was first suggested in 1934 by Fermi, and a special kind of pseudopotential is used in our work. Only valence electrons play a vital role chemically, to determine most of the chemical properties when compared to the core electrons. To remove the core electrons due to the rapid interaction with the atomic nucleus, the approximation is allowed to take advantage of treating only the valence electrons.

Generally, it is necessary to include the valence electrons, for the reason that their states overlap with the other valence electron states from neighboring atoms in forming the molecular orbital.

2.6.2 Calculating binding energies using the counterpoise method (CP)

The DFT method can be used to calculate the binding energy between different parts of a configuration This is achieved by calculating the ground state energy of the whole and then the energy of the individual components. However, these calculations are subject to errors using a DFT code such as SIESTA which uses localised basis sets that

are focused on the nuclei. When atoms are close to each other, their basis functions will overlap, which leads to the strengthening of atomic interactions, and this could affect the total energy of the system. Generally, the Basis Set Superposition Error correction (BSSE) [18] or the counterpoise correction [19] helps to solve this type of error.

Let us consider a two molecule system which are labelled as A and B; the binding energy of the interaction can be defined as:

$$\Delta E(AB) = E_{AB}^{AB} - E_A^A - E_B^B \tag{2.21}$$

Where E_{AB}^{AB} is the total energy for the dimer system A and B, and the E_A^A, E_B^B is the total energy of the total isolated components. Here the superscript denotes the basis set used in each calculation i.e. A is just the basis set of system A, B is the basis set of B and AB is the combined basis set of both A and B.

To remove the numerical errors, the energy calculations are performed in the same total basis set AB. This is achieved in SIESTA by using 'ghost' states; (basis set functions which have no electrons or protons); to evaluate the total energy of the systems A and B in the dimer basis. This is formulated by the following equation,

$$\Delta E(AB) = E_{AB}^{AB} - E_A^{AB} - E_B^{AB} \tag{2.22}$$

Here the E_A^{AB}, E_B^{AB}, is both the energy of the system A and B evaluated based on the dimer. This method provides accurate and reliable results for different systems [20][21].

2.7. Calculations in Practice

Many steps are performed to compute the transport calculations throughout this thesis, the first step is to construct the atomic configuration of the system and then choose the appropriate pseudopotentials for each element, which is distinctive for each exchange-correlation functional. Moreover, accurate calculations take a long time and use a larger memory, so it is vital to choose an appropriate basis set for every element to reduce the time and memory needed. Also, another input parameter, such as the grid fineness and density convergence tolerances, will help to ensure that the calculation is precise. One of the parameters to control the convergence is the Pulay parameter, which accelerates or maintains the stability of the convergence of the charge density in SIESTA.

The next step is to generate the initial charge density, assuming there is no interaction between atoms and the pseudopotentials are known. The self-consistent calculation begins by calculating the Hartree potential and exchange-correlation potential, as shown that in figure 2.7.1. After that, by solving the Kohn-Sham equations a new charge density is obtained, and the next iteration is started and repeated many times till the necessary convergence criteria is reached. Therefore, we get the ground state Kohn-Sham orbitals as well as the ground state energy for a given atomic conformation. For the geometric optimisation, this operation is performed in another loop, which is controlled via conjugate gradient method [22][23] to obtain the minimum ground state energy and the corresponding atomic structure. Finally, when the self-consistency has been implemented, the Hamiltonian and the density matrices are achieved. The ability to generate Hamiltonians is important as they are the key ingredient for the quantum transport calculations in the next chapter.
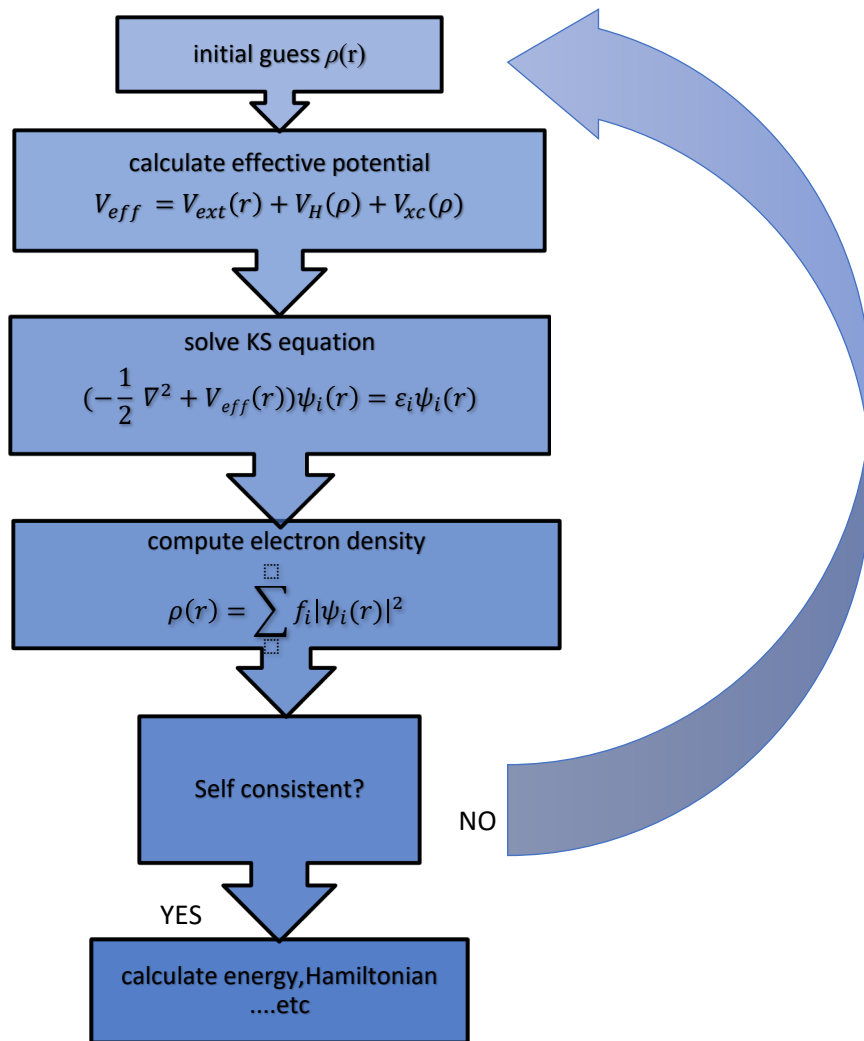
Figure 2.1: Schematic of the self-consistency process within SIESTA.

Bibliography

[1]   Soler, J. M., Artacho, E., Gale, J. D., García, A., Junquera, J., Ordejón, P. and Sánchez-Portal, D. (2002). The SIESTA method for ab initio order-N materials simulation. *Journal of Physics: Condensed Matter, 14*(11), 2745.

[2]   Parr, R. G., and W. Yang. (1989). "Density Functional Methods of Atoms and Molecules."

[3]   Gross, E.K.U and Dreizler ,R.M. (1990). Density functional theory: an approach to the quantum many-body problem.

[4] Kohn, W., & Sham, L. J. (1965). Self-consistent equations including exchange and correlation effects. *Physical review*, 140(4A), A1133.

[5] Hohenberg, P., and Kohn, W. (1964). Inhomogeneous electron gas. *Physical review*, 136(3B), B864.

[6] Argaman, N. and Makov ,G. (2000). Density Functional Theory: an introduction. *American Journal of Physics*,68(1):69-79.

[7] Martin, R.M. (2004). Electronic structure: basic theory and practical methods. *Cambridge university press.*

[8] Kohn, W., Becke, A. D. and Parr, R. G. (1996). Density functional theory of electronic structure. *The Journal of Physical Chemistry*, 100(31), 12974-12980.

[9] Born, M. and Oppenheimer, R. (1927). On the quantum theory of molecules. *Annalen der Physik*, 84(20): p. 457–484.

[10] Bartók-Pịrtay, A. (2010). The Gaussian Approximation Potential: an interatomic potential derived from first principles quantum mechanics. S*pringer Science & Business Media.*

[11] Sahni, V. (2004). The Hohenberg-Kohn Theorems and Kohn-Sham Density Functional Theory. *In Quantal Density Functional Theory* (pp. 99-123). Springer, Berlin, Heidelberg.

[12] Kohn, W. (1999).Nobel Lecture: Electronic structure of matter-wave functions and density functionals*. *Reviews of Modern Physics*,71(5): 1253-1266.

[13] Jones, R. O., & Gunnarsson, O. (1989). The density functional formalism, its applications and prospects. *Reviews of Modern Physics*, 61(3), 689.

[14] Grossman, J. C., Mitas, L. and Raghavachari, K. (1995). Structure and stability of molecular carbon: importance of electron correlation. *Physical review letters,* 75(21), 3870.

[15] Zupan, A., Blaha, P., Schwarz, K., & Perdew, J. P. (1998). Pressure-induced phase transitions in solid Si, SiO 2, and Fe: Performance of local-spin-density and generalized-gradient-approximation density functionals. *Physical Review B*, 58(17), 11266.

[16] Perdew, J. P., Burke, K. and Ernzerhof, M.(1996). Generalized gradient approximation made simple. *Physical review letters*, 77(18), 3865.

[17] Sánchez-Portal, D., Ordejon, P., Artacho, E. and Soler, J. M. (1997). Density-functional method for very large systems with LCAO basis sets. *International journal of quantum chemistry*, 65(5), 453-461.

[18]. Jansen, H. B. and Ros, P. (1969). Non-empirical molecular orbital calculations on the protonation of carbon monoxide. *Chemical Physics Letters*, 3(3), 140-143.

[19] Boys, S. F. and Bernardi, F. J. M. P. (1970). The calculation of small molecular interactions by the differences of separate total energies. Some procedures with reduced errors. *Molecular Physics*, 19(4), 553-566.

[20] Haynes, P. D., Skylaris, C. K., Mostofi, A. A. and Payne, M. C. (2006). Elimination of basis set superposition error in linear-scaling density-functional calculations with local orbitals optimised in situ. *Chemical physics letters*, 422(4-6), 345-349.

[21] Boese, A. D., Jansen, G., Torheyden, M., Höfener, S. and Klopper, W. (2011). Effects of counterpoise correction and basis set extrapolation on the MP2 geometries of hydrogen bonded dimers of ammonia, water, and hydrogen fluoride. *Physical Chemistry Chemical Physics*, 13(3), 1230-1238.

[22] Press, W. H. (2007).Numerical recipes 3rd edition: The art of scientific computing. Cambridge university press.

[23] Payne, M. C., Teter, M. P., Allan, D. C., Arias, T. A. and Joannopoulos, A. J. (1992). Iterative minimization techniques for ab initio total-energy calculations: molecular dynamics and conjugate gradients. *Reviews of modern physics*, 64(4), 1045.

[24] Penev, E., Kratzer, P. and Scheffler, M. (1999). Effect of the cluster size in modeling the H 2 desorption and dissociative adsorption on Si (001). *The Journal of chemical physics*, 110(8), 3986-3994.

Chapter 3

Theory of Quantum Transport

3.1. Introduction

In the single-molecule electronics field, one important advantage is that transport properties at the molecular scale may be controlled chemically by the design and synthesis of new types of molecules. Furthermore, understanding the electrical and thermal behaviour of the molecular junctions is a long-sought goal with the aim of designing more efficient materials. To measure the conductance through the molecule precisely, there must be reliable connections between the surface of the metal electrodes and the anchor groups of the molecule. The coupling strength between the electrodes

and the molecule is usually small in comparison to the intra- electrode and inter molecular bond strengths, which introduces a scattering process within a lead|*molecule*|lead structure. Understanding the scattering process within these junctions and molecular bridges can be obtained through Green's function method.

In this chapter, I will begin with a brief overview of how to determine the behaviour of resonances in the transmission coefficient as a function of energy by using some of the important concepts like the Breit-Wigner formula. Next, I will discuss scattering theory and introduce the Landauer formula. Following this, I will present the Green's function approach for different transport systems, such as a one-dimensional structure with an arbitrary scattering region. Finally, I will describe the general methodology to calculate the transmission coefficient *T(E)* in a molecular junction for electrons with energy *E* passing from one electrode to another.

3.2. The transmission curve features

Quantum interference is a fundamental quantum phenomena and the main characteristic of electron transport through single molecules. Some molecules have multiple paths for transporting electrons across the junction, and these paths may lead to resonances or anti-resonances. The aim of this section is to study the properties of these resonances in order to have an understanding of the transport properties that may arise in molecular junctions and devices. I will briefly demonstrate some examples of different kinds of resonances, namely Breit-Wigner resonances [1], anti-resonances [2][3] and Fano resonances[4][5].

3.2.1 Breit-Wigner resonance

The Breit –Wigner formula is a significant concept that helps to understand the behaviour of resonance in the transmission coefficient $T(E)$. When the energy of an incident electron resonates with an energy level of the molecule in the scattering region the transmission probability is expressed by a Lorentzian function, via the Breit-Wigner formula:

$$T(E) = \frac{4\Gamma_1\Gamma_2}{(E-\varepsilon_n)^2 + (\Gamma_1+\Gamma_2)^2} \qquad (3.1)$$

Through this formula, the transmission coefficient can be described by three parameters: (Γ_1, Γ_2) and (ε_n). Where Γ_1 and Γ_2 are the coupling strength of the molecular orbital to each of the electrodes, E is the energy of an electron passing through the system, and ($\Gamma_1 + \Gamma_2$) is the level broadening on resonance(resonance width). Also, ($\varepsilon_n = \lambda - \sigma$) where λ describe the eigen-energy of the molecular orbital shifted slightly by the real part of the "self-energy σ "($\sigma = \sigma_L - \sigma_R$) due to the coupling of the orbitals to the electrodes.

Within this formula, there are many components that affect the transmission coefficient. For example, when the electron resonates with the molecular orbital (e.g. when $(E = \varepsilon_n)$, electron transmission is a maximum. Also, on resonance $(E = \varepsilon_n)$, the transmission coefficient can reach a maximum of $T (E) = 1$, if $\Gamma_1 = \Gamma_2$ (e.g. a symmetric molecule attached symmetrically to identical leads). Moreover, the width of the resonance depends on the sum $\Gamma_1 + \Gamma_2$, so when the coupling to the electrode is weak, the resonance is sharp and vice versa. This formula is valid in the case that the level spacing of the isolated molecule is larger than the width of the resonance ($\Gamma_1 + \Gamma_2$).

3.2.2 Anti-resonance

The transmission probability curve has one important feature, which is the anti-resonance or (off-resonance) . This phenomenon can appear when the energy of the incoming electron E coincides with the eigenenergy E_n of one of the two branches, as shown in figure (3.1). A destructive interference occurs when the amplitudes of propagating waves along the two branches sum to zero at the nodal points.
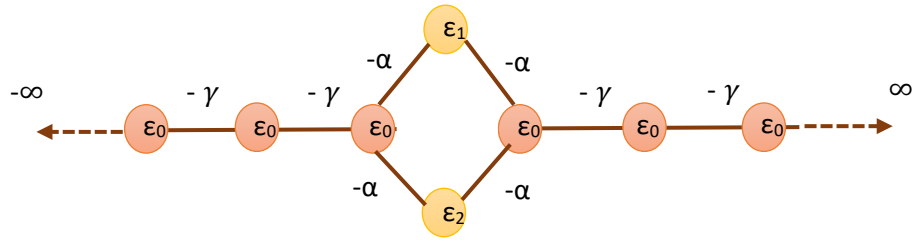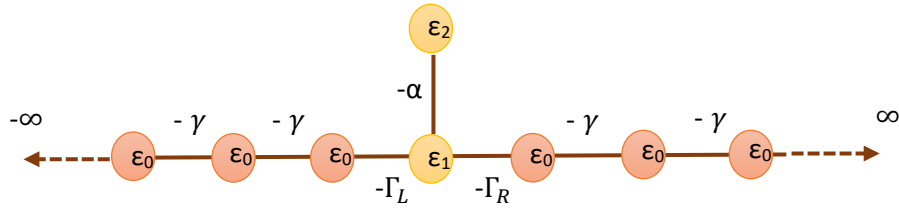

Figure 3.1: Tight binding model of anti-resonance, when two semi-finite one-dimensional chain coupled to the scattering region.

3.2.3 Fano resonance

A Fano resonance is usually signaled by a resonance showing the typical Fano line shape, which is a resonance followed by an anti-resonance. This appearance is due to the interference between a discrete state (e.g. a pendant group) which is weakly coupled to the continuum state, and this gives an asymmetric line shape. We can observe this phenomenon for instance, when a pendant group is connected to a central backbone by the coupling of (α) which is considered to be more weakly coupled than the coupling to the open system Γ_L and Γ_R as shown in figure (3.2). The width of a Fano resonance become narrow by varying the (α) coupling. To calculate the transmission coefficient, we can use the formula in equation (3.2):

$$T(E) = \frac{4\Gamma_L\Gamma_R}{(E-\varepsilon_n)^2 + (\Gamma_L + \Gamma_R)^2} \qquad (3.2)$$

where $\varepsilon_n = \varepsilon_1 + \frac{\alpha^2}{E-\varepsilon_2}$. For small α, the resonance condition when $E = \varepsilon_n$ can be satisfied when $E \approx \varepsilon_1$ and $E \approx \varepsilon_2$. On the other hand, when $E = \epsilon_2$ this generates a an anti-resonance, which is close to resonance at $E \approx \varepsilon_2$. These two features combine to give the characteristic Fano line shape [5][6].

Figure 3.2: Tight binding model of Fano-resonance, when two semi-finite one-dimensional chain coupled to the scattering region of site energy ε1 by hopping elements$\Gamma_L$andΓ_R. An extra energy level ε2 is coupled to the scattering area by hopping element –α.

3.3 Scattering matrix

To provide an understanding of the transport properties in scattering theory, calculating the scattering-matrix is useful. We can obtain it by solving the time-independent Schrödinger equation for an electron approaching from the left electrode

$$\psi_j = \frac{A}{\sqrt{v_l}} e^{ik_l j} + \frac{B}{\sqrt{v_l}} e^{-ik_l j} \qquad (3.3)$$

where A and B are the amplitudes of the two ingoing and outgoing waves travelling to the left and right, respectively, here v is the group velocity.

The current per unit energy that it carries is:

$$I_{left} = |A^2| - |B^2| \qquad (3.4)$$

For the right electrode:

$$\psi_j = \frac{C}{\sqrt{v_r}} e^{ik_r j} + \frac{D}{\sqrt{v_r}} e^{-ik_r j} \qquad (3.5)$$

$$I_{right} = |C^2| - |D^2| \qquad (3.6)$$

where C and D are the amplitudes of the two ingoing and outgoing waves travelling to the right and left, respectively.

Since the bond current satisfies the relation $I_l = I_r$

$$|A^2| - |B^2| = |C^2| - |D^2| \qquad (3.7)$$

ie

$$|A^2| + |D^2| = |B^2| + |C^2| \qquad (3.8)$$

This states that the incoming current is equal to outgoing current, and the wave functions for the left electrode and right respectively are:

$$Ae^{ikj} + Be^{-ikj} \qquad (3.9)$$

$$Ce^{ikj} + De^{-ikj} \qquad (3.10)$$

To match the outgoing with incoming coefficients, we construct the s-matrix, which is also known as the scattering matrix:

$$\begin{bmatrix} B \\ C \end{bmatrix} = \begin{bmatrix} S_{11} & S_{12} \\ S_{21} & S_{22} \end{bmatrix} \begin{bmatrix} A \\ D \end{bmatrix} \qquad (3.11)$$

Then

$$B = S_{11}A + S_{12}D \tag{3.12}$$

$$C = S_{21}A + S_{22}D \tag{3.13}$$

If $A = 1$ and $D = 0$, then $B = r, C = t$. Where r is the amplitude of the reflected wave

due to an incoming wave from the left and t is the amplitude of the transmitted wave

$$\begin{bmatrix} B \\ C \end{bmatrix} = \begin{bmatrix} S_{11}A \\ S_{21}A \end{bmatrix} \tag{3.14}$$

The physical meaning of S_{11} is (r) and S_{21} is (t) which is the reflection and transmission,

respectively.

If $D = 1$ and $A = 0$:

$$\begin{bmatrix} B \\ C \end{bmatrix} = \begin{bmatrix} S_{12}D \\ S_{22}D \end{bmatrix} \tag{3.15}$$

Where S_{12} is (t') and S_{22} is (r') which is the reflection and transmission respectively.

Then:

$$S = \begin{pmatrix} S_{11} & S_{12} \\ S_{21} & S_{22} \end{pmatrix} = \begin{pmatrix} r & t' \\ t & r' \end{pmatrix} \tag{3.16}$$

Since the bond current satisfies the relation $I_l = I_r$

$$|A^2| - |B^2| = |C^2| - |D^2| \tag{3.17}$$

And therefore as a consequence of charge conservation,

$$|A^2| + |D^2| = |B^2| + |C^2| \tag{3.18}$$

where the incoming current from both leads is $|A^2| + |D^2|$ and the outgoing current

into both leads is $|B^2| + |C^2|$, therefore

$$(A^* \quad D^*)\begin{pmatrix} A \\ D \end{pmatrix} = (B^* \quad C^*)\begin{pmatrix} B \\ C \end{pmatrix} \tag{3.19}$$

Taking the Hermitian conjugate of the scattering matrix equation (3.11) yields $(B^* \quad C^*) = (A^* \quad D^*)S^\dagger$ and substituting these into equation (3.19)

$$(A^* \quad D^*)S^\dagger S \begin{pmatrix} A \\ D \end{pmatrix} = (B^* \quad C^*)\begin{pmatrix} B \\ C \end{pmatrix} \tag{3.20}$$

This shows that $S^\dagger S$ is the unit matrix a (I) and therefore S is unitary:

$$\begin{pmatrix} r^* & t^* \\ t^* & r^* \end{pmatrix}\begin{pmatrix} r & t' \\ t & r' \end{pmatrix} = \begin{pmatrix} 1 & 0 \\ 0 & 1 \end{pmatrix} \tag{3.21}$$

In terms of scattering theory:

$$|r^2| + |t^2| = 1 \ \Rightarrow R + T = 1 \tag{3.22}$$

$$|r'^2| + |t'^2| = 1 \ \Rightarrow R^2 + T^2 = 1 \tag{3.23}$$

where T and R represent the transmission and reflection.

3.4 The Landauer formula

The Landauer formula [7][8] describes the transport of non-interacting electrons for a scattering region in terms of a transmission coefficient and a Fermi distribution of the connected electrodes. To illustrate this method, consider a scattering region connected to two electrodes (leads) as sketched in figure (3.3). The leads are assumed to be ballistic conductors, i.e. conductors with no scattering, and thus the transmission probability equals one. Each lead, in turn, is coupled to a reservoir where all inelastic processes take place. These electrodes supply the system with electrons, and these reservoirs have a slightly different chemical potential $(\mu_L - \mu_R = E > 0)$ which leads to the passing of electrons from left to the right, and let the temperature be equal to zero ($T=0\ K$) [6].
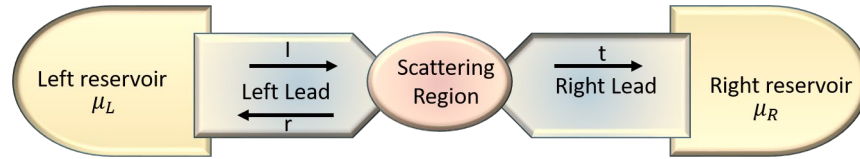

Figure 3.3: A scattering region connected to two electrodes. The electrodes are connected to a reservoir with chemical potential μ_L and μ_R .

To calculate the current for this system moving from left to right in a particular range and similarly from right to left, the current generated by the chemical potential difference is:

$$\delta I = e\, v_g \frac{\partial n}{\partial E} \delta E = e\, v_g \frac{\partial n}{\partial E}\, (\mu_L - \mu_R) \qquad (3.24)$$

where the electron charge is e, the group velocity is v_g and $\frac{\partial n}{\partial E}$ is the density of states

per unit length and can be defined by the chemical potential of the contact.

$$\frac{\partial n}{\partial E} = \frac{\partial n}{\partial k}\frac{\partial k}{\partial E} = \frac{\partial n}{\partial k}\frac{1}{v_g \hbar} \qquad (3.25)$$

In one dimension, when having a spin dependency $\frac{\partial n}{\partial k} = \frac{1}{2\pi}$, substituting into

Equation (3.25) gives:

$$\frac{\partial n}{\partial E} = \frac{1}{v_g h} \qquad (3.26)$$

Equation (3.26) becomes:

$$\delta I = \frac{2e}{h}\left(\mu_L - \mu_R\right) \qquad (3.27)$$

$$\delta I = \frac{2e^2}{h}\delta V \qquad (3.28)$$

where the voltage in the reservoir generated by the difference in the potential is δV. When considering a scattering region, the current passing through the scatterer to the right lead is written as:

$$\delta I = \frac{2e^2}{h}T(E)\delta V \qquad (3.29)$$

$$G = \frac{\delta I}{\delta V} = \frac{2e^2}{h}T\,(E) \qquad (3.30)$$

In the absence of a scattering region:

$$G = \frac{2e^2}{h} \qquad (3.31)$$

$$G_0 = \frac{2e^2}{h} \qquad (3.32)$$

where G_0 is the quantum of conductance and it is $G_0 = \left(\frac{2e^2}{h}\right) = 77 \ \mu S$.

In the presence of the scattering region, the conductance will be:

$$G = \frac{2e^2}{h} \ T \ (E) \tag{3.33}$$

$$G = G_0 T(E) \tag{3.34}$$

Equation (3.34) is called the Landauer formula for a one-dimensional system and the current is given by.

$$I = \frac{2e}{h} \int_{-\infty}^{\infty} dE \ T(E)[f_L(E) - f_R(E)] \tag{3.35}$$

where $e = -|e|$, h is Plank's constant, and $T \ (E \ )$ is the transmission coefficient for the electron passing from one lead to the other via the molecule, and

$$f_{L(R)}(E) = \frac{1}{e^{\frac{E-\mu_{L(R)}}{k_B T}} + 1} \tag{3.36}$$

$f_{L(R)}$ Is the Fermi-Dirac distribution function, $\mu_{L(R)}$ is the chemical potential of the left (right) reservoir respectively, T is the temperature, and k_B is Boltzmann's constant.

If the voltage V is applied on the left and right reservoirs symmetrically, then $\mu_L = E_F + \frac{eV}{2}$ and $\mu_R = E_F + \frac{eV}{2}$, this means at zero temperature and finite voltage the current will be:

$$I = \left(\frac{2e}{h}\right) \int_{E_F - \frac{eV}{2}}^{E_F + \frac{eV}{2}} dE \ T(E) \tag{3.37}$$

The electrical conductance at zero voltage and the finite temperature is:

$$G = \frac{I}{V} = G_0 \int_{-\infty}^{\infty} dE \, T(E) \left(-\frac{df(E)}{dE} \right)_{\mu=E_F} \tag{3.38}$$

The above integral represents a thermal average of the transmission function $T(E)$ over an energy window of width $k_B T$ where T is the temperature.

3.5 Green's Function

This Green function is an essential tool for studying the transport properties of different nanoscale structures [9]. In the beginning, I will discuss how to construct the Green's function for different situations. Then I will briefly present how to connect the Green's functions of these separable lattices together to construct the Green's function of the whole system using the Dyson equation.

3.5.1 Green's function of a doubly infinite chain

This section illustrates the Green's function of the doubly infinite chain for electrodes. In this case, these electrodes are described as a perfect crystalline structure that is periodic in the direction of transport, the z-direction, as shown in figure (3.4).
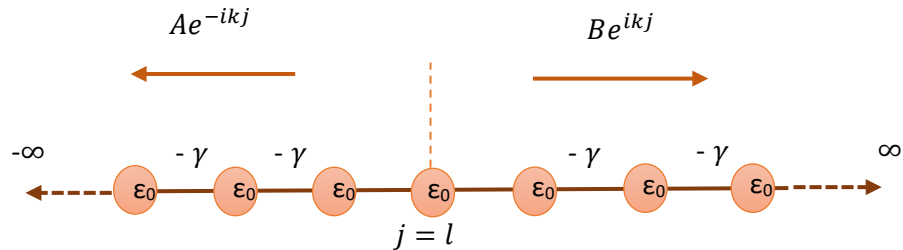

Figure 3.4: Tight binding representation of one-dimensional infinite chain with on-site energies ε_0 and couplings $-\gamma$.

The time-independent Schrödinger equation is:

$$(E - H)|\psi\rangle = 0 \tag{3.39}$$

The Green's function of a system described by a Hamiltonian (H) can be defined as the solution of:

$$(E - H)G = I \tag{3.40}$$

The formal solution to this equation would be given by:

$$G = (E - H)^{-1} \tag{3.41}$$

where G is the retarded Green's function (g_{jl}) describes the response of a system at a point j due to a source at l

$$(E - H)g_{jl} = \delta_{jl} \tag{3.42}$$

where δ_{jl} is Kronecker delta, which is equal to 1 if $j = l$ and zero otherwise.

The Green's function for an infinite system

$$\varepsilon_0 g_{jl} - \gamma g_{j+1,l} - \gamma g_{j-1,l} + \delta_{jl} = E g_{jl} \tag{3.43}$$

If the solutions are:

$$g_{jl} = \begin{cases} A e^{ikj} & j \geq l \\ B e^{-ikj} & j \leq l \end{cases} \tag{3.44}$$

where A and B represent the amplitudes of the two waves coming from the right and left respectively. Because a Green's function is continuous at $j = l$; as a result, I can write that:

$$g_{jl}|_{j=l} = \begin{cases} Ae^{ikj} & j \geq l \\ Be^{-ikj} & j \leq l \end{cases} \tag{3.45}$$

Therefore: $g_{ll} = \alpha$. Applying these results to Eq (3.43) and considering the energy for the infinite system I obtain:

$$(\varepsilon_0 - E)\alpha - \gamma\alpha e^{ik} - \gamma\alpha e^{ik} = -1 \tag{3.46}$$

$$\gamma\alpha(2cosk - 2e^{ik}) = -1 \tag{3.47}$$

$$\alpha = \frac{1}{2i\gamma sink} \tag{3.48}$$

$$\alpha = \frac{1}{i\hbar v} \tag{3.49}$$

where v is the group velocity and $\hbar v(E) = 2\gamma sink(E)$. The result of equation (3.49) and (3.45) combines to get the Green's function for the double infinite chain [10][11]:

$$g_{jl}^{\infty} = \frac{e^{ik|l-j|}}{i\hbar v} \tag{3.50}$$

where g_{jl}^{∞} represents the retarded Green's function, which describes the two outgoing waves from the source j= l .

3.5.2 Green's function of a semi-infinite one-dimensional chain

To derive the Green's function of a semi-infinite chain consider the problem of a doubly infinite chain, and introduce an appropriate boundary condition in order to obtain the Green's function for this system as shown in figure (3.5).

This infinite chain must terminate at a given point *P+1, so* all points *P+1 ≥P* are missing which means the Green's function is eliminated at the site *P+1*. This can be accomplished by adding a wave function to a double infinite Green's function.
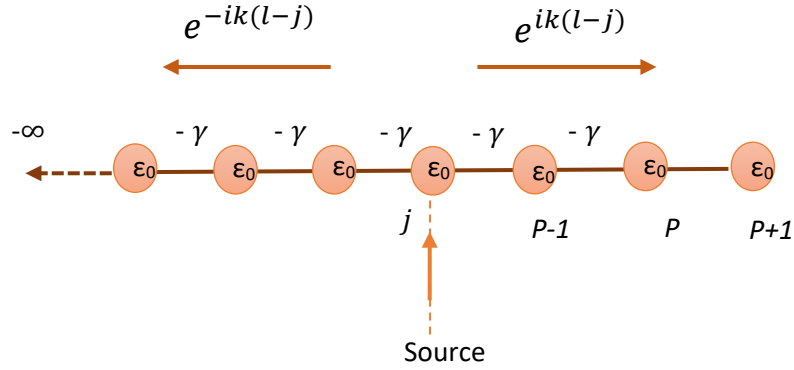

Figure 3.5: tight-binding model of a semi-infinite one-dimensional chain with on-site energies ε_0 , couplings $-\gamma$, and j denote the labels of the sites in the chain.

The general Green's function is written as:

$$g_{jl} = g_{jl}^{\infty} + \psi_{jl} \tag{3.51}$$

The appropriate wave function is simply:

$$\psi_{jl} = Ae^{-ikl} \tag{3.52}$$

$$A = -\frac{e^{-ikj}}{i\hbar v}e^{2ik(P+1)} \tag{3.53}$$

The Green's function terminated at point (P) due to source at (l =j) is:

$$g_{Pj} = \frac{e^{ikp}e^{-ikj} - e^{-ikj}e^{2ik(P+1)}e^{-ikP}}{i\hbar v} \tag{3.54}$$

From the boundary condition where j= l =P thereby:

$$g_{Pj} = \frac{-e^{ik}}{\gamma} e^{ik(P-J)} \qquad (3.55)$$

The Green's function for site $j=P$ due to source on site $l = P$

$$g_{p,p} = -\frac{e^{ik}}{\gamma} \qquad (3.56)$$

which is the surface Green's function.

3.5.3 One dimensional scattering

To obtain the Green's function of the whole structure, we must connect the Green's functions of the separable system together. Let us consider the case where we have two semi-finite one -dimensional leads connected to each other by a coupling of $(-\gamma)$ with site energy of (ε_0) and coupled by hopping element $-\alpha$, as presented in figure (3.6). Scattering problems could be reduced to this simple form of one-dimensional system, by deriving the transmission and reflection coefficient of an electron travelling from the left to the right lead through the scattering region.
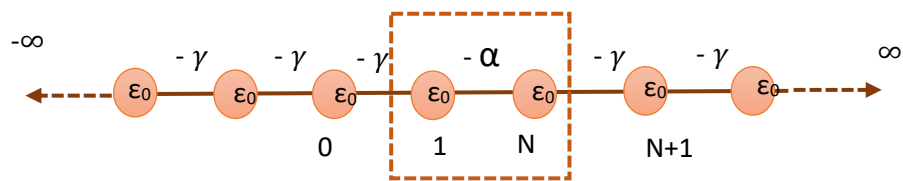

Figure 3.6: Tight binding model of a 1-D scattering region attached to a one-dimensional lead.

The Hamiltonian takes the form of an infinite matrix, is given by:

$$
\begin{pmatrix}
\ddots & -\gamma & 0 & 0 & 0 & 0 \\
-\gamma & \varepsilon_0 & -\gamma & 0 & 0 & 0 \\
0 & -\gamma & \varepsilon_0 & \alpha & 0 & 0 \\
0 & 0 & \alpha & \varepsilon_0 & -\gamma & 0 \\
0 & 0 & 0 & -\gamma & \varepsilon_0 & -\gamma \\
0 & 0 & 0 & 0 & -\gamma & \ddots
\end{pmatrix}
= \begin{pmatrix} H_L & V_c \\ V_c^\dagger & H_R \end{pmatrix}
\tag{3.57}
$$

where H_L and H_R the Hamiltonians of the left lead and right lead, respectively, and the coupling to connect these leads is V_c.

In order to compute the scattering amplitudes, calculating the Green's function of this problem is necessary, which is written as:

$$
G = (E - H)^{-1}
\tag{3.58}
$$

The retarded Green's function has been defined above as equation (3.50), and the semi-infinite Green's function is given by equation (3.55). In the case of decoupled leads where α=0 the total Green's function is written as:

$$
g = \begin{pmatrix} \dfrac{-e^{ik}}{\gamma} & 0 \\ 0 & \dfrac{-e^{ik}}{\gamma} \end{pmatrix} = \begin{pmatrix} g_L & 0 \\ 0 & g_{LR} \end{pmatrix}
\tag{3.59}
$$

The Green's function for the coupled system can be obtained using the Dyson equation, which is:

$$
G = (g^{-1} - V)^{-1}
\tag{3.60}
$$

Clearly:

$$
\begin{pmatrix} 0 & V_c \\ V_c^\dagger & 0 \end{pmatrix} = \begin{pmatrix} 0 & -\alpha \\ -\alpha^* & 0 \end{pmatrix}
\tag{3.61}
$$

By solving Dyson's equation leads to the Green's function of this system which is:

$$G = \frac{1}{\gamma^2 e^{-2ik} - \alpha^2} \begin{pmatrix} \gamma e^{-ik} & -\alpha \\ -\alpha & \gamma e^{-ik} \end{pmatrix} \tag{3.62}$$

After finding the Green's function for this system, the scattering coefficients can be obtained by using the Fisher-Lee relation, which relates the scattering amplitudes of a scattering problem to the Green's function of the same problem.

The Fisher-Lee relation is:

$$r = i\hbar v G_{0,0} - 1 \tag{3.63}$$

$$t = i\hbar v G_{0,N+1} \, e^{ik} \tag{3.64}$$

The coefficients correspond to a particle travelling from the left, and the same procedure could be done in order to compute these coefficients for a particle travelling from the right.

$$T = |t|^2 \tag{3.65}$$

$$R = |r|^2 \tag{3.66}$$

So, after constructing the full scattering matrix and by using the Landauer formula, we can calculate the zero-bias conductance of the system.

3.5.4 Transport through an arbitrary scattering region

In this section, I will derive the most general formula for the transmission probability for an arbitrarily shaped scattering structure. Consider a nanoscale system, as shown in figure (3.7), with a scattering region of sites (1) to (N) and Hamiltonian H connected to one-dimensional electrodes from both sides. Each atom in the leads has on-site energy (ε_0) with a coupling of $(-\gamma)$.
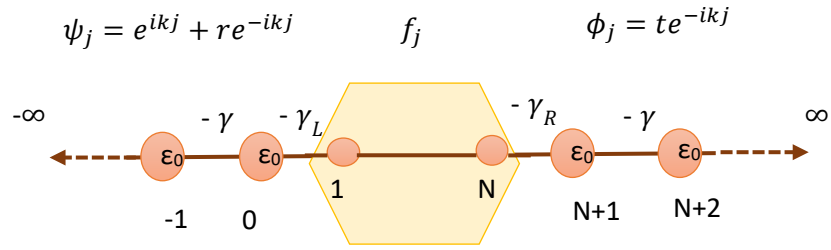
Figure 3.7: Tight binding model of arbitrary scattering region attached to the one-dimensional lead.

The wave functions for this system representing each of:

First, the left side is:

$$\psi_j = e^{ikj} + re^{-ikj} \tag{3.67}$$

Secondly, the right side is

$$\phi_j = te^{ikj} \tag{3.68}$$

Lastly, the scattering region is

$$f_j \tag{3.69}$$

The Schrödinger equation in these regions could be written as respectively:

For j ≤ -1:

$$\varepsilon_0\psi_j - \gamma\psi_{j-1} - \gamma\psi_{j+1} = E\psi_j \tag{3.70}$$

When j=0

$$\varepsilon_0\psi_0 - \gamma\psi_{-1} - \gamma_l f_1 = E\psi_0 \tag{3.71}$$

For scattering region:

When j=1

$$\sum_{l=1}^{N} H_{1l} f_l - \gamma_l \psi_0 = E f_1 \tag{3.72}$$

For $2 \leq j \leq N\text{-}1$

$$\sum_{l=1}^{N} H_{jl} f_l = E f_j \tag{3.73}$$

For j=N

$$\sum_{l=1}^{N} H_{Nl} f_l - \gamma_R \phi_{N+1} = E f_N \tag{3.74}$$

For j=N+1

$$\varepsilon_0 \phi_{N+1} - \gamma \phi_{N+2} - \gamma_R f_N = E \phi_{N+1} \tag{3.75}$$

For $j \geq N+2$

$$\varepsilon_0 \gamma \phi_j - \gamma \phi_{j-1} - \gamma \phi_{j+1} = E \phi_j \tag{3.76}$$

When j=0 in equation (3.71) and (3.72):

$$\gamma_L f_1 = \gamma \psi_1 \tag{3.77}$$

When j=N+1 in equation (3.76) and (3.77):

$$\gamma_R f_N = \gamma \phi_N \tag{3.78}$$

Constructing $\psi_0 \ and \ \phi_{N+1}$:

$$\psi_0 = \frac{\gamma_L}{\gamma_0} e^{ik} f_1 - (2i)(sink) e^{ik} \tag{3.79}$$

$$\phi_{N+1} = \frac{\gamma_R}{\gamma} e^{ik} f_N \tag{3.80}$$

Then: $|\psi\rangle = \Sigma |f\rangle + |S\rangle$

$$\begin{pmatrix} -\gamma_L \psi_0 \\ -\gamma_R \phi_{N+1} \end{pmatrix} = \begin{pmatrix} \Sigma_L f_1 \\ \Sigma_R f_N \end{pmatrix} + \begin{pmatrix} 2\gamma_L e^{ik} sink \\ 0 \end{pmatrix} \tag{3.81}$$

Where the self- energies to the left and right lead are Σ_L and Σ_R, respectively. By

solving equation (3.81), we achieve:

$$|\psi\rangle = \Sigma_g|\psi\rangle + |S\rangle \tag{3.82}$$

$$|\psi\rangle = (I - \Sigma_g)^{-1}|S\rangle \tag{3.83}$$

$$\begin{pmatrix} -\gamma_L\psi_0 \\ -\gamma_R\phi_{N+1} \end{pmatrix} = \frac{1}{det}\begin{pmatrix} 1 - \Sigma_R g_{NN} & \Sigma_L g_{1N} \\ -\gamma_R g_{N1} & 1 - \Sigma_L g_{11} \end{pmatrix}\begin{pmatrix} S_L \\ 0 \end{pmatrix} \tag{3.84}$$

Therefore, the transmission (t) could be obtained as:

$$t = \frac{\gamma_L\gamma_R}{\gamma} e^{ik}e^{-ikN}(2isink)(\frac{g_{N1}}{det}) \tag{3.85}$$

Where the determinant is det$=1 - \Sigma_R g_{NN} - \Sigma_L g_{11} + \Sigma_L\Sigma_R(g_{11}g_{NN} - g_{1N}g_{N1})$

The transmission probability is $T(E) = |t|^2$ which could be written as:

$$T(E) = 4(\frac{\gamma_R^2 sink}{\gamma})(\frac{\gamma_L^2 sink}{\gamma})\left|\frac{g_{N1}}{det}\right|^2 \tag{3.86}$$

$$T(E) = 4\Gamma_R\Gamma_L\left|\frac{g_{N1}}{det}\right|^2 \tag{3.87}$$

This is the most general solution to calculate the transmission probability for any

scattering region connected with the same electrodes.

Bibliography

[1]   Breit, G., & Wigner, E. (1936). Capture of slow neutrons. Physical review, 49(7), 519.

[2] Ke, S. H., Yang, W. and Baranger, H. U. (2008). Quantum-interference-controlled molecular electronics. Nano letters, 8(10), 3257-3261.

[3]   Stadler, R. (2009). Quantum interference effects in electron transport through nitrobenzene with pyridil anchor groups. Physical Review B, 80(12), 125401.

[4]   Papadopoulos, T. A., Grace, I. M. and Lambert, C. J. (2006). Control of electron transport through Fano resonances in molecular wires. Physical review b, 74(19), 193306.

[5]   Lambert, C. J. (2015). Basic concepts of quantum interference and electron transport in single-molecule electronics. Chemical Society Reviews, 44(4), 875-888.

[6] Cuevas, J. C. and Scheer, E. (2010). Molecular electronics: an introduction to theory and experiment.

[7] Rolf Landauer. (1957)."Spatial variation of currents and fields due to localized scatterers in metallic conduction." *IBM Journal of research and development* 1(3): 223-231.

[8] Landauer, R. (1987). Electrical transport in open and closed systems. *Zeitschrift für Physik B Condensed Matter,* 68(2-3), 217-228.

[9] Claughton, N. R., Leadbeater, M., & Lambert, C. J. (1995). Theory of Andreev resonances in quantum dots. *Journal of Physics: Condensed Matter,* 7(46), 8757.

[10] Datta, S. (1997). Electronic transport in mesoscopic systems. Cambridge university press.

[11] Economou, E. N. (2006). Green's functions in quantum physics (Vol. 7). Springer Science & Business Media.

Chapter 4

Electrical molecular switch addressed by chemical stimuli

This work was carried out in collaboration with experimental groups in Marseille and de Lille universities and demonstrates the conductance switching of benzo-bis(imidazole) molecules upon protonation and shows how it depends on the lateral functional groups. The results presented in this chapter were published in "Electrical molecular switch addressed by chemical stimuli" *Nanoscale, 2020, 12, 10127.*

4.1. Introduction

Molecular electronics exploits the rich variety of organic molecules to create custom-designed molecular devices for applications in future electronics. The desired

function should be encoded in the molecules, which are then connected to electrodes. Among the numerous functional molecules found in the literature, the most striking examples of molecular devices are arguably molecular switches, i.e. molecules which exist as at least two stable isomers, whose electronic properties can be controllably and reversibly modified by external stimuli[1]. These switches should be distinguished from molecules where a stochastic conductance switching is observed (e.g. for uncontrollable switching driven by the electric field, or electrode/molecule instabilities) [2-6]. For conformational switches, the 3D structure of the molecule is modified by the isomerization reaction (stereoisomerization). The cis-trans isomerization induced by light of the azobenzene molecule [7-12], photoisomerization of diarylethene [13-16] and hydrogen tautomerization reaction in phtalocyanine [17] are well-known examples of such switches. In redox switches, the electronic properties depend on the modification of the charge state of the molecules [18-22] through oxidation or reduction depending on the position of the electrochemical potential with respect to the HOMO-LUMO gap of the molecule. It is also possible to control the conductance of molecular junctions by the photo-population of excited state [23-26]. In this case, upon resonant illumination, the electrons photo-injected in the LUMO increase the current through the molecular junctions. In contrast to conformational and redox switches, this effect is not persistent, vanishing rapidly when the excitation is turned off.

Several demonstrations of an alternative approach, the electronic conductance modulation by pH in molecular junctions, have been reported [27-31]. However, these results are puzzling about which state (protonated or deprotonated) leads to the higher conductance of the molecules. For example, the conductance value in the junction can be modified by the protonation or deprotonation of the anchor group of the molecule grafted on a metal surface (electrode). Single molecules of alkanes terminated with

diamine or dicarboxylic-acid groups measured by scanning tunnelling microscope break-junction (STM-BJ) in a pH controlled solution show higher conductance at pH = 13 (deprotonated) than at pH = 1 (protonated) [28]. For these authors, the basic (pH = 13) or acid (pH = 1) environment of the molecular junction modifies the chemical specie of the anchoring group: NH_2 and COO^- in basic environment and NH_3^+ and COOH in acidic medium. The NH_2 and COO^- species enhance the coupling strength between the molecule and the gold electrode, compared to the NH_3^+ and COOH species formed in acidic environment. In the specific case of dithiol terminated alkanes, no significant variation of the conductance was observed with the pH. The same behaviours were also observed for diacid oligo(phenylene ethylene) Langmuir Blodgett films characterized by scanning tunnelling microscope (STM)[30] with a higher conductance (ratio ≈ 7) for the deprotonated form (COO-Au bond at pH = 11.4) than for the protonated form (COOH-Au bond at pH = 5.9). This difference of conductance was interpreted by the chemical modification of the anchoring group with pH as in Ref [28], but also by the formation of lateral H bonds between neighbouring molecules in the films. For these systems, the higher conductance was obtained for the deprotonated form ($G_{depro} > G_{pro}$). More recently, STM-BJ measurements of 4,4'-vinylenedipyridine connected between Ni electrodes showed a conductance switch attributed to change in the electrode/molecule coupling upon protonation, and moreover, the pH required to switch the conductance can also be tuned by the applied electrochemical potential[32]. Protonation and deprotonation of a π-conjugated molecular system bridged in a molecular junction can also modify the conductance. Oligoaniline derivatives connected into gaps in single-walled carbon nanotubes exhibit conductance variations of around one decade between the protonated form (pH = 3) and deprotonated form (pH = 11) and this variation was reversible during 5 cycles[29]. The higher conductance

was obtained for the protonated form. In Another system, a multi-sensitive molecule (pH and light) based on a spyropiran derivative and characterized by STM-BJ shows an increase of the conductance by a factor about 2 after protonation of the spyropiran in the open form [31]. For these π-conjugated molecular systems, the higher conductance was obtained for the protonated form ($G_{pro} > G_{depro}$).

It can also be mentioned that an inversion of the rectifying effect in diblock molecular diodes by protonation was observed by STM [27]. This inversion was explained by a modification of the dipolar moment of the molecule with the protonation that induces a diminution of the HOMO and LUMO energies. Consequently, the conduction occurs by resonant tunnelling through the HOMO before the protonation and through the LUMO after. This last result shows that the protonation or deprotonation of the molecule can modify the molecular orbital energy of the molecule addressed in a molecular junction. A similar influence of the protonation on the LUMO position was reported for SAMs, in which the protonation of the terminal carboxylic acid groups converts back and force the molecular junctions between a resistor and a rectifying diode [33]. Protonation has also been used, in combination, with light irradiation to block the spiropyran molecule in its merocyanine isomer and avoiding its spontaneous back switching to the sypopyran form [34]. Finally, protonation has been used to induce destructive-quantum-interference in diketopyrrolopyrrole derivative, leading to a reversible decrease of the conductance (1 order of magnitude) upon protonation [35].
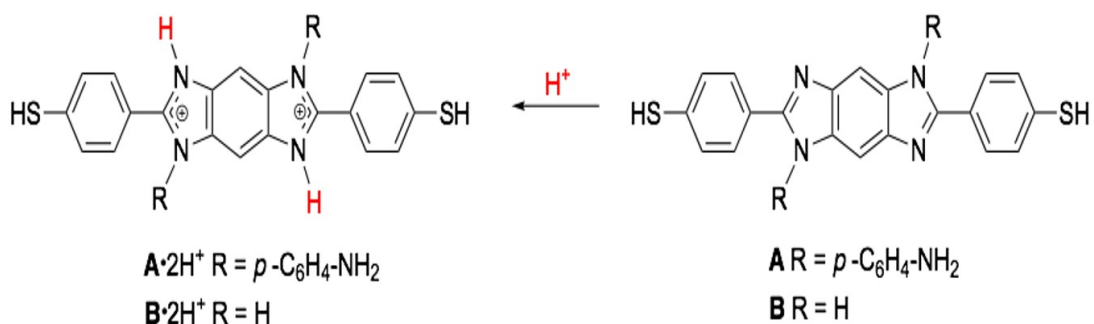
Figure 4.1. Benzo-bis(imidazole) derivatives **A** and **B**, and protonation

Benzo-imidazole derivatives are known molecules which are sensitive to pH, exhibiting a different absorption and/or emission signatures depending on their protonation states [36]. Benzo-bis(imidazole) molecules, have been recently investigated as precursors of modular fluorescent probes polymers, [37-38] or Janus bis(carbene)s and transition metal complexes [39]. They are also very attractive acidochromic systems because of the presence of two localized π-subunits that can be tuned by reversible protonation to become delocalized [40]. Thus, protonation of these molecules led to a bathochromic effect ($\Delta\lambda = 13$ nm) that can be explained by the stabilization of the positive charges (colour change from yellow to orange) [41]. This prompted us to introduce the –SH anchoring group on the benzobis(imidazole) core for grafting such a molecule on gold surfaces in order to evaluate their pH-sensitive switch properties (Figure 4.1). Here, this work demonstrates that the pH effect on the molecule conductance can be controlled by side chain chemistry. A benzo-bis(imidazole) derivative molecule shows a higher conductance in the neutral case ($G_{neu}>G_{pro}$) when laterally functionalized by amino-phenyl groups (molecule **A**), while we observe the reverse case ($G_{pro}>G_{neu}$) for the H-substituted molecule (molecule **B**), figure (4.1). The molecular conductance was measured at 3 scale lengths: self-assembled monolayers

(SAM) on flat Au surface, about one hundred molecules grafted on Au nanodots (NMJ: nanodot molecule junction) and single molecule by mechanically controlled break junction (MCBJ). The conductances were measured by C-AFM in the two former cases. The 3 approaches give the same trends. These results are supported by theoretical calculations and we conclude that these opposite behaviours depend on the position of the HOMO resonances relative to the Fermi energy of the electrodes.

4.2. Methods:

4.2.1 Single-molecule in the gas phase :

"The first principles ab-initio calculations carried out using the Gaussian density functional code [41]. The geometries of molecules **A** and **B** were optimized using density functional theory in the framework of the B3LYP functional[42], the 6-311g basis set and the GDISS optimization algorithm[43]. The influence of pH through proton exchanges at the molecular level is not simple to simulate with the interplay of dielectric and solvation effects[44]. Another issue for the modelling is the presence of a counter ion (here Cl^-) at a random position in order to equilibrate the total charge of the system[45]. To co pe with this issue, a cluster model has been used as defined in Ref [46]. For each molecule (**A** and **B**) and their protonation states, the HOMO-LUMO gap, the electron affinity (EA) and the ionization potential (IP) has been calculated" . [Note, this calculation was done by *C. Krzeminski*]

4.2.2 Nanodot molecule junctions:

Nanodot molecule junctions (NMJ) is an approach used with conducting atomic force microscopy (C-AFM) to measure the molecular junction conductance or the current–voltage characteristics. This method used an array (<10 nm) made from hundreds of molecules fabricated by electronic lithography on single-crystal gold nanodots embedded in Si substrate. Each time the C-AFM tip scanning the array of NMJs, the current (at a given voltage) is recorded. After that, from these C-AFM images, the current or conductance histograms can be extracted and repeating this process at different bias allow the measurement of 2D histograms of the current-voltages (I-V) curves [50,51,52].

4.2.3 Metal/molecule/metal junction

To calculate the electron transport through these molecules when a metal/molecule/metal junction is formed, I attach the optimized geometry of the molecule to gold via the thiol anchor groups. In this case, I bind the terminal sulfur atom to a hollow site on a (111) gold surface and the optimum Au-S distance is calculated to be 2.3Å. The hydrogen atom contacted to the sulfur is removed. An extended molecule is then constructed to consist of 6 layers of (111) gold each containing 25 atoms. Using the DFT code SIESTA [47], a Hamiltonian describing the extended molecule is generated using the following parameterization. A double-ζ plus polarization orbitals basis set, energy cut off=150 Rydbergs, and the GGA exchange-correlation functional [48]. To calculate the protonated form, we control the charge on the counter ions (Cl-) via the atomic basis set. The zero-bias transmission coefficient

T(E) is then calculated as a function of the electron energy (E) using this Hamiltonian, via the GOLLUM code [49]. This is then used to evaluate the conductance and electrical current via the Landauer formula.

$$G = \frac{2e^2}{h} \int_{-\infty}^{\infty} dE \ T(E) \left(\frac{df(E)}{dE}\right)$$

Where, f(E) is the Fermi-Dirac distribution, e is the electronic charge and h is Planck's constant. The electrical current is evaluated,

$$I = \frac{2e}{h} \int_{-\infty}^{\infty} dE T(E)[f_L(E) - f_R(E)]$$

Where f_L and f_R are the Fermi-Dirac distributions in the right and left lead respectively.

4.3. Results and discussion

4.3.1. Electrical characterization

The electrical current through molecules **A** and **B** was measured by my collaborators in Marseille and de Lille universities using three methods, the details of which can be found in ref[52]. As an example, I show the results for the current measured using the nanodot molecule junction. The current histograms at 200 mV for both the molecules and in both states (protonated and neutral) are presented in figure 4.2. These histograms show a shift of the distribution between the protonated and neutral NMJs, with higher current for the neutral molecule **A** ($G_{neu}(A) > G_{pro}(A)$) and a decrease of the current for the neutral molecule **B** ($G_{pro}(B) > G_{neu}(B)$).
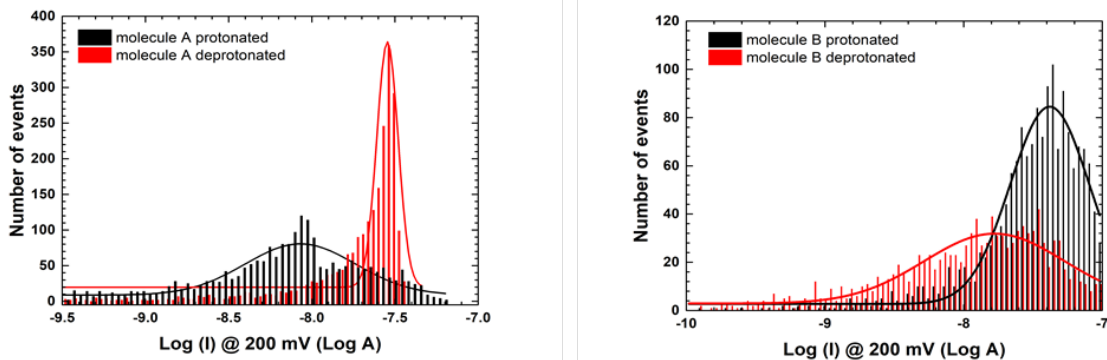
Figure 4.2 Histograms of the current at a fixed bias (200 mV) measured by C-AFM on **(a)** a molecule **A** after protonation in black and for neutral molecules in red; **(b)** molecule **B** after protonation in black and for neutral molecules in red.

A summary of all the measured current values is shown in table 1, and shows that the other methods follow the same trend as the NMJ measurement. However, molecule **A** could not be measured at the single molecule level using the MCBJ method. The values of the switching ratios are shown in table 2 and has values in the range 3-10, the theoretical predicted ratios are also in good agreement using the method defined later.

Table 1. Current values for molecules **A** and **B** measured at 3 scale lengths by 3 approaches (n.m: not measured)

	A_{dep}	A_{pro}	B_{dep}	B_{pro}
MCBJ	n.m	n.m	1.4×10^{-10}A	9.1×10^{-10}A
NMJ	2.9×10^{-8}A	8.5×10^{-9}A	1.7×10^{-8}A	4.2×10^{-8}A
SAM/Au^{TS}	1.4×10^{-8}A	1.5×10^{-9}A	3.2×10^{-10}A	2.0×10^{-9}A

Table 2. Switching ratio for molecules A and B measured at 3 scale lengths by 3 approaches and theoretical calculations. (n.m: not measured)

	MCBJ	NMJ	SAM/Au^{TS}	Theory
A (G_{deprot}/G_{prot})	n.m.	3.4	9.3	6
B (G_{prot}/G_{deprot})	4.5-6.5	2.5	6.3	15

4.3.2 Modeling molecule in gas phase

The first step in modelling is to calculate the optimized geometries, the electron affinity (EA), the ionization potential (IP) and the HOMO-LUMO gap for molecules **A** and **B** in the neutral and protonated forms. Figure (4.3) shows the optimized geometries for molecules **A** and **B**, the centre of the molecule (imidazole) and the two phenyl groups remain planar. The length of both molecules **A** and **B** are 18.9Å which is the distance between the terminating sulfur atoms.

For the unprotonated state of molecule **A,** the dihedral angle between the alanine rings and imidazole is near 90°. For both molecules, the imidazole ring presents the most accessible protonation sites with the presence of two non-hydrogenated nitrogen atoms. The introduction of an HCl molecule leads to the formation of N-H bond characterized by a bond length of 1.0764 Å. For the molecules **A and B** up to two protonation degrees can be foreseen with the protonation of the nitrogen atoms as shown in Figure (4.3).
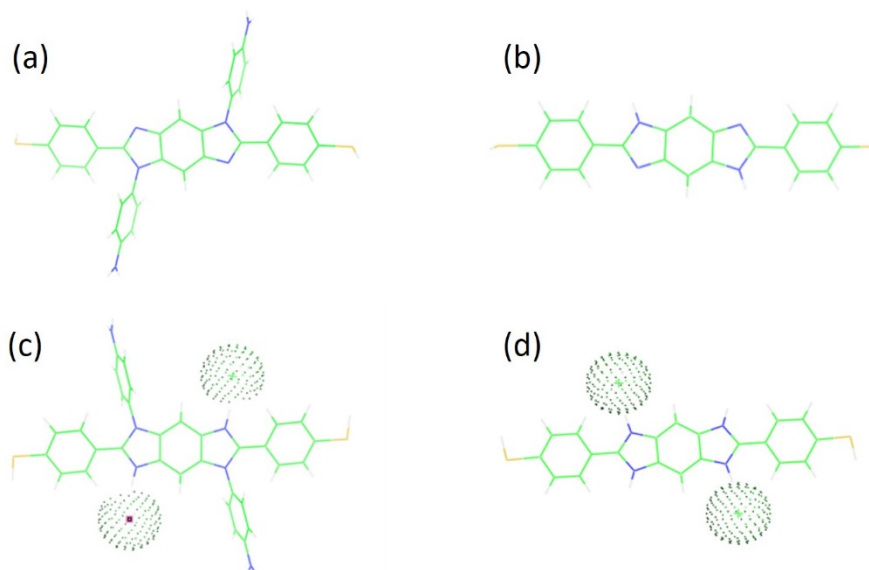
Figure 4.3. Optimized geometries of **(a)** unprotonated molecule **A**, **(b)** unprotonated molecule **B**, **(c)** protonated molecule **A** with two protons and **(d)** protonated molecule **B** with two protons. [Note, this calculation was done by C. Krzeminski]

4.3.2.1 Energy Levels :

Figure 4.4 shows the results for the electronic properties of molecules A and B, and these demonstrate that protonation tends to reduce the HOMO–LUMO gap of the molecules and increases the IP and EA. The Ionization Potential (IP) and the Electron Affinity (EA) can provide a more accurate calculation of the HOMO and LUMO energy levels. If E(N) is the ground state energy of the neutral molecule, where N is the number of electrons, the energy associated with the addition of one electron E(N+1) is called the electron affinity (EA). Also, the energy associated with removing one electron E(N-1) is called the ionization energy or potential (IP). Where IP=E(N-1)-E(N) and EA=E(N)-E(N+1). Furthermore, the energy gap or the HOMO-LUMO gap is E_g = IP-EA , where IP= - E_{HOMO} and EA= - E_{LUMO}.

When molecule A and B are protonated and the number of the HCL is increased from 1 to 2, the HOMO-LUMO gap decreases and the HOMO and LUMO levels move to lower energy. This means that as the number of sites are protonated the energy levels shift. For molecule A, which has 4 protonation sites the energy gap is constant after 2 sites have been protonated, as seen in Figure(4.4-a). Therefore the extra protonation on the amine sites does not change the electronic properties of the molecule. Therefore, in the following transport calculations I use two chlorine atoms. An important point here in the case of the neutral molecules is that while the HOMO-LUMO gap is similar for both (3.8eV), the ionization potential of **B** is 0.5eV lower than **A**.
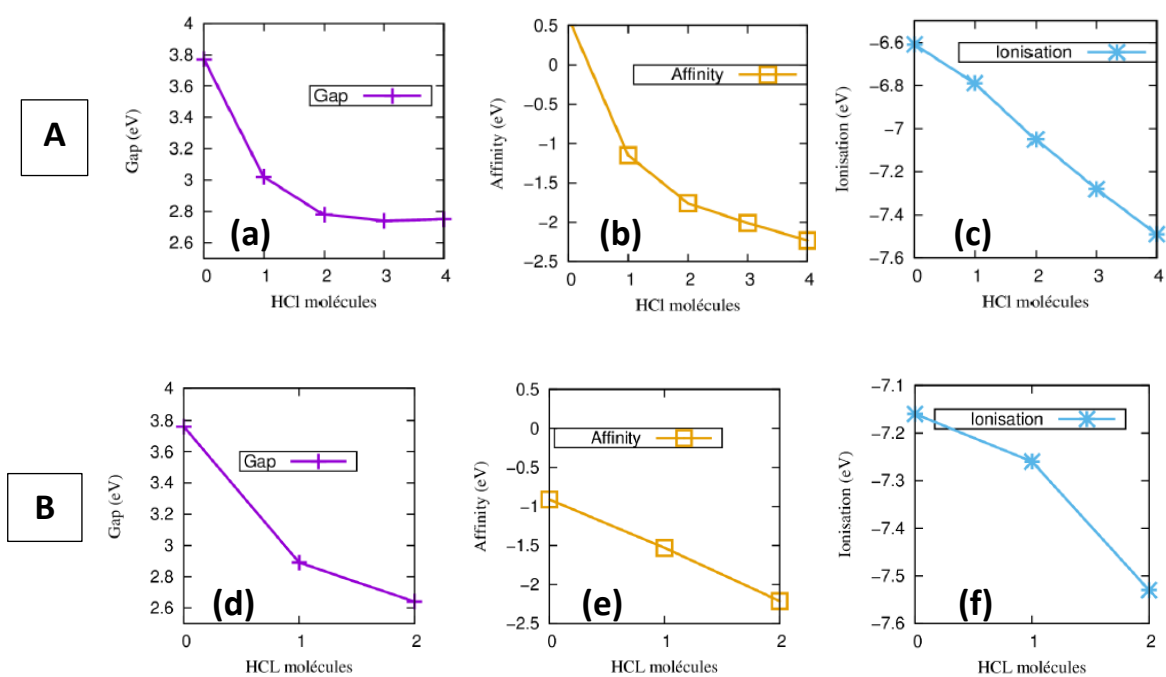
Figure 4.4. Evolution of **(a)** the HOMO-LUMO gap, **(b)** electron affinity and **(c)** ionization potential of molecule **A** versus the protonation state. Evolution of **(d)** the HOMO-LUMO gap, **(e)** electron affinity and **(f)** ionization potential of molecule **B** versus the protonation state. [Note, this calculation was done by *C. Krzeminski*]

4.3.3. Modeling electron transport in metal/molecule/metal junctions

To explain the measured switching behaviour, electron transport calculations were performed through the two molecules when attached to gold electrodes. First, I examine the simple comparison between the deprotonated molecules **A** and **B** when they are attached to gold electrodes as described in the methods section. Figure (4.5) shows the calculated conductance through molecules **A** and **B** for the geometry given in figure (4.8). Here, the HOMO resonances of the two molecules lie at similar positions relative to the SIESTA predicted Fermi Energy $E_F{}^0 = 0eV$ and give comparable conductance values. This disagrees with the calculated behaviour in the gas phase where the HOMO level of **B** lies at lower energy. This can be attributed to the thiol anchor groups

pinning the HOMO close to the Fermi energy and explains why the results don't match the measured conductance which shows molecule **A** has a higher conductance in the neutral forms (Table 1).
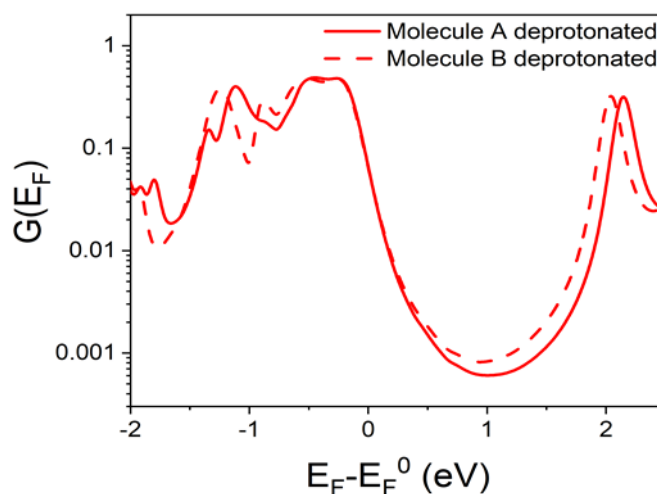
Figure 4.5. Electrical conductance of the deprotonated molecules **A** and **B**.

4.3.4. Transport through NH2 anchor groups in Molecule A

Another thing to consider in the junction formation of these molecules is the fact that Molecule **A** contains NH_2 groups which can also act as anchor groups and may lead to coupling to gold electrodes. I calculate T(E) for this geometry where the N-Au distance is 2.4 nm (figure 4.6). The resulting transmission shows that the off-resonance values in the HOMO-LUMO gap (i.e. $1E-6G_0$ at 0eV) are much lower than the equivalent molecule binding through the thiols ($\sim 1E-3G_0$). At the Fermi energy, the value is approximately 3 orders of magnitude lower. This is due to the phenyl ring rotation between the NH_2 groups and the central core, which is approximately 90°, and suggest that these groups play a minimal role in the electron transport.
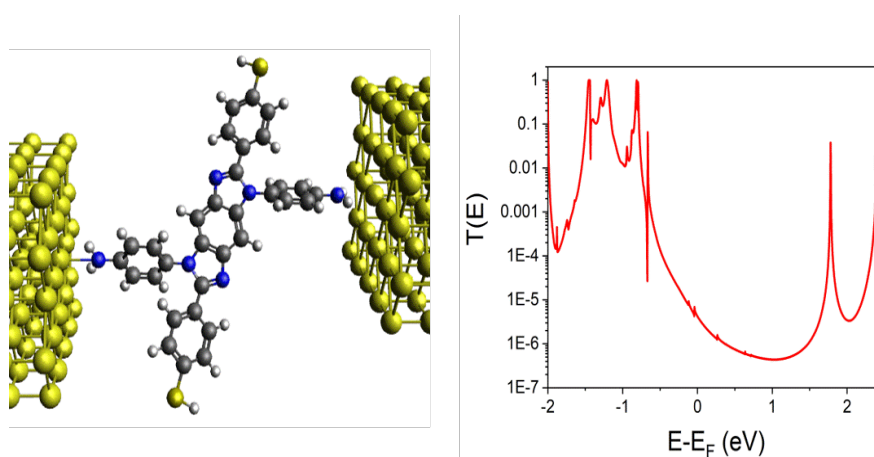
Figure 4.6. (left) Geometry of molecule **A** contacted to gold electrodes through the NH_2 groups and (right) the corresponding zero-bias transmission coefficient T(E).
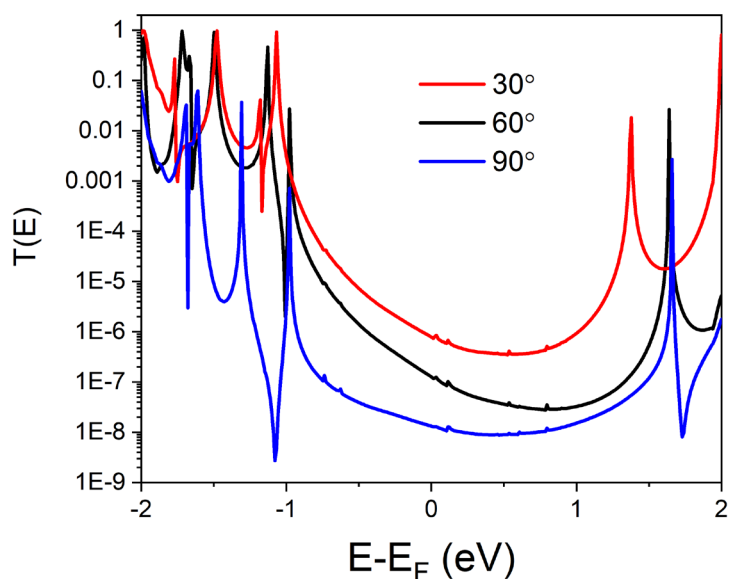
Figure 4.7. zero-bias transmission coefficient T(E) for different rotation angle of the phenyl ring between the NH_2 groups and the central core of molecule A.

The modelling of protonation of the molecules is more complex than the neutral versions, as adding hydrogen atoms at the nitrogen sites, causes the molecule to become charged. Therefore, counter ions, (which here are chlorine ions) are needed to balance the charge i.e. making the added hydrogen atoms H^+ and the chlorine atoms Cl^-. To achieve this within SIESTA requires analysis of the electron distribution using a Mulliken population analysis. To form a Cl^- ion requires the number electrons on the chlorine atom to increase by one (Here I define N as the number of electrons added to the chlorine atom).

This calculation was performed by varying the distance between the counter ions and the hydrogen atom of the protonation site on both molecule **A** and **B** and evaluating the number of electrons N on the Cl atom. The results are shown in table 3, and the optimum distance for the maximum value of N (0.6 and 0.5 for **A** and **B** respectively) occurs at

a CL-H distance of 3Å, it also shows the sensitivity of the charge distributions in these calculations to the position of the counter ions. Even for the optimum case, the number of the electrons on the chlorine atom is still not equal to one. However, the chlorine atom plays no direct part in the electron transport through the junction, it is only responsible for the electrostatic control of charge, therefore the basis set of chlorine can be utilized to control the behaviour of the counter ions. The basis sets in SIESTA (which are pseudo atomic orbitals) are defined by the cut-off radius, this is the value beyond which the wavefunction is zero. Here I set the Cl-H distance to be 3Å and increase the values of the cutoff radii, the results show in table 4 that for longer basis sets the number of electrons N on the chlorine atom increases and reaches a value of one when the radius is > 8 Bohr. I then compare the behaviour of the transmission coefficient for the protonated version of molecule **B** when the charge on the counter ion is controlled via this method. Figure (4.8) shows that when there are no counter ions the LUMO resonance lies directly at the Fermi energy (0eV) as is expected for a charged system (cyan line). The addition of the counter ions shifts the position of the Fermi energy into the middle of the HOMO-LUMO gap and the amount of shift is controlled by the value of N on the counter ions. Here N=0.7 (blue line) and N=1.0 (black line).

Table 3: The values of N by Varying the distance of the counter ions on both molecules **A** and **B**.

Distance (Å)	N (Molecule **A)**	N (Molecule **B)**
1	0.1	0.1
2	0.5	0.4
3	0.6	0.5
4	0.5	0.4
5	0.4	0.4

Table 4: The increase in value of N determined by a Mulliken population analysis on the chlorine counter ions by varying the cut-off radius in the basis set for molecules **A** and **B**.

Cutoff Radii (Bohr)	N (Molecule **A**)	N (Molecule **B**)
n=3 0 2 3.826 3.17 n=3 1 2 4.673 3.419	0	0
n=3 0 2 5.826 5.172 n=3 1 2 5.673 5.419	0	0.7
n=3 0 2 6.826 6.172 n=3 1 2 6.673 6.419	0	0.7
n=3 0 2 7.826 7.172 n=3 1 2 7.673 7.419	1	1
n=3 0 2 8.826 8.172 n=3 1 2 8.673 8.419	1	1
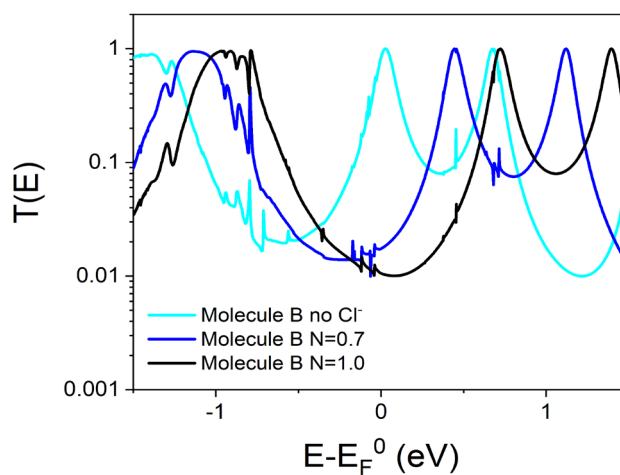
Figure 4.8 Transmission coefficient T(E) for the protonated molecule **B** when the are no Cl- counter ions (cyan), when the number of electron N on the Cl atom =0.7 (blue) and when N=1 (black).

Having established the methods, I now compare the transport behaviour of molecules

A and **B** in their protonated and deprotonated forms to explain the switching effect seen

in the experimental measurements. I calculate the transport properties for identical contacting geometries as shown in figure (4.9). The resulting transmission curves T(E) in figure (4.9) show the gap between the HOMO and LUMO resonances is approximately 2 eV. Molecule **A** in the neutral (deprotonated) form shows that the DFT predicted Fermi energy (E_F^0=0eV) lies close to the HOMO resonance and gives a conductance value of $0.06G_0$. Upon protonation, the HOMO-LUMO gap is decreased and the position of the Fermi energy lies in the middle of the gap. The value of conductance decreases to $0.01G_0$ in agreement with the trend shown in the NMJ measurement of figure 4.2.
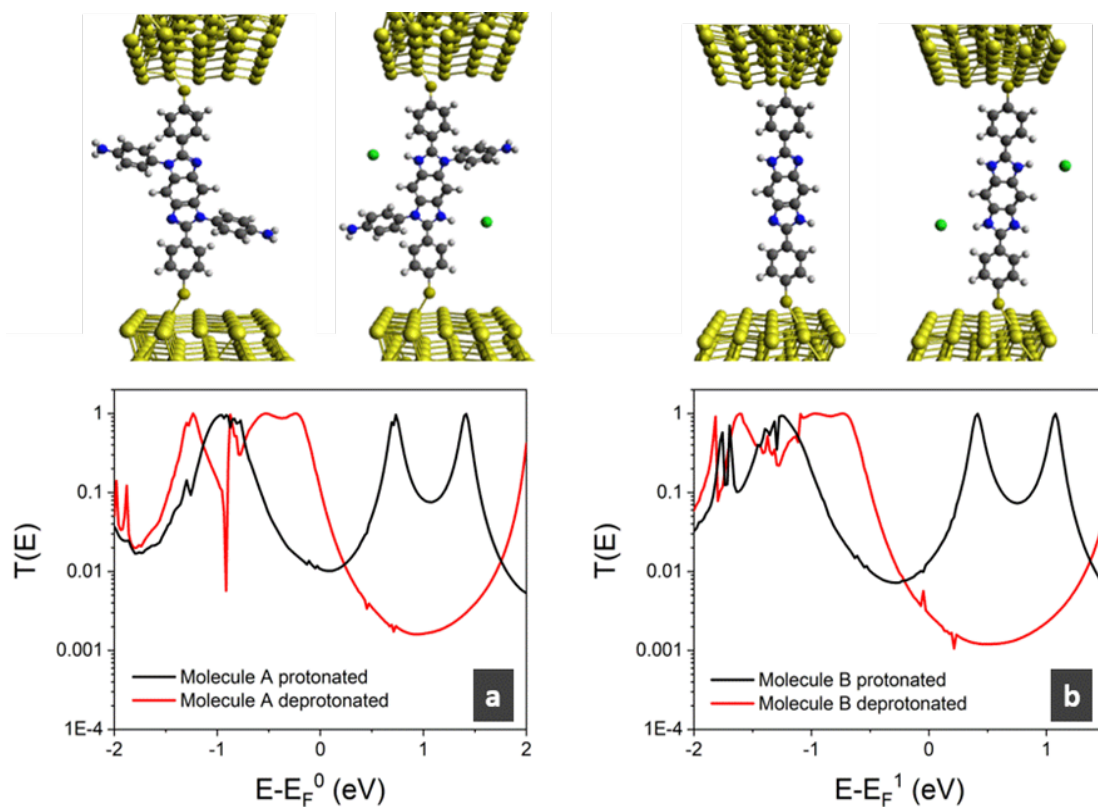
Figure 4.9. Zero bias transmission coefficient T(E) for molecule A (a) and molecule B (b) in a linear geometry for the protonated and deprotonated forms.

For molecule **B**, I find that the DFT calculation positions the Fermi energy close to the HOMO, leading to a similar transmission for Molecule **A** figure 4.5. However, the calculated IP of molecule **B** is larger than **A** (meaning the HOMO is at lower energy). Figure 4.4 shows this difference to be ~0.5eV, and therefore I shift the Fermi energy by this amount and define $E_F^1 = E_F^0 + 0.5eV$. The value of the conductance for the deprotonated case at E_F^1 is $0.002G_0$. Protonation again decreases the HOMO-LUMO gap, but now the transmission is higher at $E-E_F^1 = 0eV$ and the conductance increases to a value of $0.03G0$, again in agreement with the measured trend of figure (4.2). The conductance ratio for molecule A $G_{deprot}/G_{prot} = 6$ and $G_{prot}/G_{deprot} = 15$ for molecule **B** are in excellent agreement with our measured ratios in Table 2. Thus, the changing behaviour on protonation between molecule A and B can be attributed to the difference in the relative position of the HOMO resonance with respect to the Fermi energy.

4.3.5. Tilt angle

One final thing to consider is the geometry of the molecule in the junction. The measured thickness [52] of these molecules when they form SAMs shows that Molecule **A** has a smaller thickness (1.3nm) than **B** (1.9nm) which suggests the molecule **A** is tilted while **B** stands upright. Figure 4.10 calculates T(E) for a tilt angle of 60° away from the normal (the gold-gold separation is now 1.4nm). The result shows the same trend to the upright geometry in figure 4.9, with the transmission decreasing when the molecule is protonated. Suggesting that the geometry is not important.
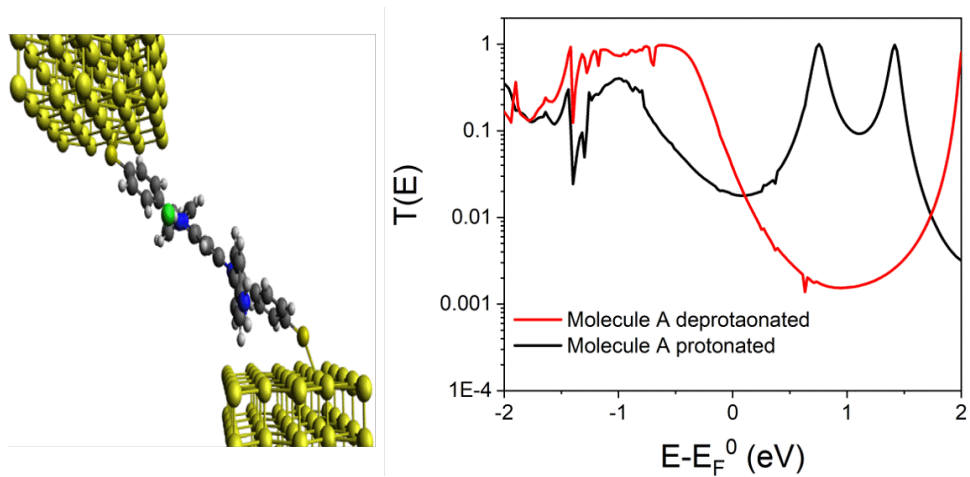
Figure 4.10. Zero bias transmission coefficient T(E) for molecule A tilted at an angle of 60° away from the normal.
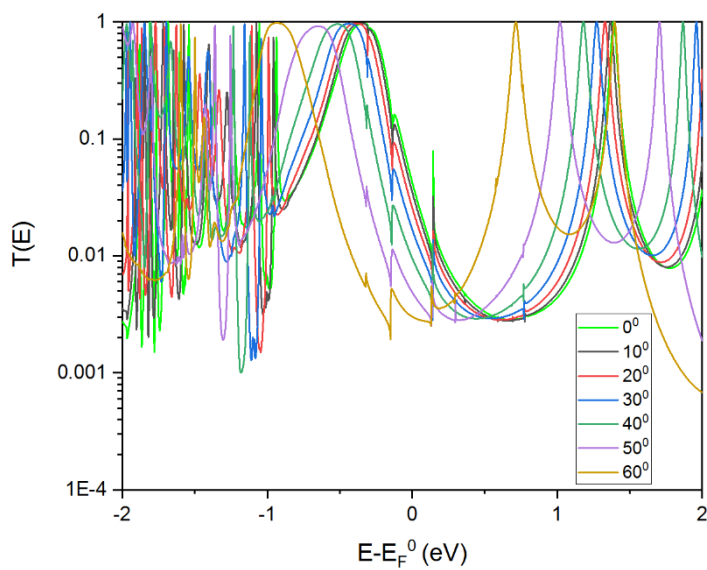

Figure 4.11. Zero bias transmission coefficient T(E) for molecule A(protonated) in different tilted angles.

4.4. Conclusion

A multi-scale characterization of the electron transport through molecular junction upon protonation/deprotonation demonstrates that the conductance switching depends on the lateral functional groups. The molecular conductances were measured at 3 scale lengths: self-assembled monolayers on flat Au surfaces, about hundred molecules grafted on Au nanodots (measured by C-AFM in these two cases) and single-molecule by mechanically controlled break junction, and. The 3 approaches demonstrate that the pH effect on the molecule conductance can be controlled by side chain chemistry. A benzo-bis(imidazole) molecule shows a higher conductance in the neutral state ($G_{neu}>G_{pro}$) when laterally functionalized by amino-phenyl groups, while the reverse case ($G_{pro}>G_{neu}$) for the H-substituted molecule is observed. These results are understood with the help of theoretical calculations and I conclude that these opposite behaviours depend on the electronic coupling between molecules and electrodes and the relative alignment of the Fermi energy with the molecular orbitals.

Bibliography

1.   van der Molen, S. J.; Liljeroth, P., Charge transport through molecular switches. *J Phys Condens Matter* **2010,** *22*, 133001.

2.   Ramachandran, G. K.; Hopson, T. J.; Rawlett, A. M.; Nagahara, L. A.; Primak, A.; Lindsay, S. M., A bond-fluctuation mechanism for stochastic switching in wired molecules. *Science* **2003,** *300* (5624), 1413-1416.

3.   Van Der Molen, S. J.; Vegte, H. V. D.; Kudernac, T.; Amin, I.; Feringa, B. L.; Wees, B. J. V., Stochastic and photochromic switching of diarylethenes studied by scanning tunnelling microscopy. *Nanotechnology* **2005,** *17* (1), 310-314.

4.   Jang, S.-Y.; Reddy, P.; Majumdar, A.; Segalman, R. A., Interpretation of stochastic events in single molecule conductance measurements. *Nano Lett* **2006,** *6* (10), 2362-7.

5.   Battaglini, N.; Klein, H.; Hortholary, C.; Coudret, C.; Maurel, F.; Dumas, P., STM observation of a single diarylethene flickering. *Ultramicroscopy* **2007,** *107* (10), 958-962.

6.   Moore, A.; Mantooth, B.; Donhauser, Z.; Yao, Y.; Tour, J.; Weiss, P., Real-time measurements of conductance switching and motion of single oligo (phenylene ethynylene) molecules. *J. Am. Chem. Soc* **2007,** *129* (34), 10352-10353.

7.   Bellini, B.; Ackermann, J.; Klein, H.; Grave, C.; Dumas, P.; Safarov, V., Light-induced molecular motion of azobenzene-containing molecules: a random-walk model. *J Phys Condens Matter* **2006,** *18*, S1817-S1835.

8.   Katsonis, N.; Lubomska, M.; Pollard, M. M.; Feringa, B.; Rudolf, P., Synthetic light-activated molecular switches and motors on surfaces. *Progress in Surf. Sci.* **2007,** *82*, 407-434.

9.   Ferri, V.; Elbing, M.; Pace, G.; Dickey, M. D.; Zharnikov, M.; Samorì, P.; Mayor, M.; Rampi, M. A., Light-Powered Electrical Switch Based on Cargo-Lifting Azobenzene Monolayers. *Angew. Chem. Int. Ed.* **2008,** *47* (18), 3407-3409.

10. Kumar, A. S.; Ye, T.; Takami, T.; Yu, B.-C.; Flatt, A. K.; Tour, J. M.; Weiss, P. S., Reversible Photo-Switching of Single Azobenzene Molecules in Controlled Nanoscale Environments. *Nano Lett.* **2008,** *8* (6), 1644-1648.

11. Mativetsky, J. M.; Pace, G.; Elbing, M.; Rampi, M. A.; Mayor, M.; Samori, P., Azobenzenes as Light-Controlled Molecular Electronic Switches in Nanoscale Metal-Molecule-Metal Junctions. *J. Am. Chem. Soc.* **2008,** *130* (29), 9192-9193.

12. Smaali, K.; Lenfant, S.; Karpe, S.; Oçafrain, M.; Blanchard, P.; Deresmes, D.; Godey, S.; Rochefort, A.; Roncali, J.; Vuillaume, D., High On−Off Conductance Switching Ratio in Optically-Driven Self-Assembled Conjugated Molecular Systems. *ACS Nano* **2010,** *4* (4), 2411-2421.

13. Irie, M., Diarylethenes for Memories and Switches. *Chem Rev* **2000,** *100* (5), 1685-1716.

14. Katsonis, N.; Kudernac, T.; Walko, M.; Van der Molen, S.; Van Wees, B.; Feringa, B., Reversible conductance switching of single diarylethenes on a gold surface. *Adv. Mat.* **2006,** *18* (11), 1397-1400.

15. Kronemeijer, A. J.; Akkerman, H. B.; Kudernac, T.; Van Wees, B. J.; Feringa, B. L.; Blom, P. W. M.; De Boer, B., Reversible Conductance Switching in Molecular Devices. *Adv. Mater.* **2008,** *20* (8), 1467-1473.

16. van der Molen, S. J.; Liao, J.; Kudernac, T.; Agustsson, J. S.; Bernard, L.; Calame, M.; van Wees, B. J.; Feringa, B. L.; Schönenberger, C., Light-controlled conductance switching of ordered metal-molecule-metal devices. *Nano Letters* **2009,** *9* (1), 76-80.

17. Liljeroth, P.; Repp, J.; Meyer, G., Current-induced hydrogen tautomerization and conductance switching of naphthalocyanine molecules. *Science* **2007,** *317*, 1203-1206.

18. Gittins, D. I.; Bethell, D.; Schiffrin, D. J.; Nichols, R. J., A nanometer-scale electronic switch consisting of a metal cluster and redox-addressable groups. *Nature* **2000,** *408*, 67-69.

19. Liu, Z.; Yasseri, A. A.; Lindsey, J. S.; Bocian, D. F., Molecular memories that survive silicon device processing and real-world operation. *Science* **2003,** *302*, 1543-1545.

20.   Roth, K. M.; Yasseri, A. A.; Liu, Z.; Dabke, R. B.; Malinovskii, V.; Schweikart, K.-H.; Yu, L.; Tiznado, H.; Zaera, F.; Lindsey, J. S.; Kuhr, W. G.; Bocian, D. F., Measurements of electron-transfer rates of charge-storage molecular monolayers on Si(100). Towards hybrid molecular/semiconductor information storage devices. *J. Am. Chem. Soc.* **2003,** *125* (2), 505-517.

21.   Mahapatro, A.; Ying, J.; Ren, T.; Janes, D., Electronic Transport through Ruthenium-Based Redox-Active Molecules in Metal− Molecule− Metal Nanogap Junctions. *Nano Letters* **2008,** *8* (8), 2131-2136.

22.   Liao, J.; Agustsson, J. S.; Wu, S.; Schönenberger, C.; Calame, M.; Leroux, Y.; Mayor, M.; Jeannin, O.; Ran, Y.-F.; Liu, S.-X.; Decurtins, S., Cyclic Conductance Switching in Networks of Redox-Active Molecular Junctions. *Nano Lett* **2010,** *10* (3), 759-764.

23.   Zhou, J.; Wang, K.; Xu, B.; Dubi, Y., Photoconductance from Exciton Binding in Molecular Junctions. *J Am Chem Soc* **2017,** *140* (1), 70-73.

24.   Morteza Najarian, A.; Bayat, A.; McCreery, R. L., Orbital Control of Photocurrents in Large Area All-Carbon Molecular Junctions. *J Am Chem Soc* **2018,** *140* (5), 1900-1909.

25.   Pourhossein, P.; Vijayaraghavan, R. K.; Meskers, S. C. J.; Chiechi, R. C., Optical modulation of nano-gap tunnelling junctions comprising self-assembled monolayers of hemicyanine dyes. *Nat Commun* **2018,** *7,* 11749.

26.   Najarian, A. M.; McCreery, R. L., Long-Range Activationless Photostimulated Charge Transport in Symmetric Molecular Junctions. *ACS Nano* **2019,** *13* (1), 867-877.

27.   Morales, G. M.; Jiang, P.; Yuan, S.; Lee, Y.; Sanchez, A.; You, W.; Yu, L., Inversion of the rectifying effect in diblock molecular diodes by protonation. *J Am Chem Soc* **2005,** *127* (30), 10456-10457.

28.   Chen, F.; Li, X.; Hihath, J.; Huang, Z.; Tao, N. J., Effect of anchoring groups on single-molecule conductance: comparative study of thiom-, amine-, and carboxylic-acid-terminated molecules. *J. Am. Chem. Soc.* **2006,** *128* (49), 15874-15881.

29.   Guo, X.; Small, J. P.; Klare, J. E.; Wang, Y.; Purewal, M. S.; Tam, I. W.; Hong, B. H.; Caldwell, R.; Huang, L.; O'Brien, S.; Yan, J.; Breslow, R.; Wind, S. J.; Hone, J.; Kim, P.; Nuckolls, C., Covalently bridging gaps in single-walled carbon nanotubes with conducting molecules. *Science* **2006,** *311*, 356-359.

30.   Ballesteros, L. M.; Martín, S.; Cortés, J.; Marqués-González, S.; Higgins, S. J.; Nichols, R. J.; Low, P. J.; Cea, P., Controlling the Structural and Electrical Properties of Diacid Oligo(Phenylene Ethynylene) Langmuir–Blodgett Films. *Chem. Eur. J.* **2013,** *19* (17), 5352-5363.

31.   Darwish, N.; Aragonès, A. C.; Darwish, T.; Ciampi, S.; Díez-Pérez, I., Multi-Responsive Photo- and Chemo-Electrical Single-Molecule Switches. *Nano Lett* **2014,** *14* (12), 7064-7070.

32.   Brooke, R. J.; Szumski, D. S.; Vezzoli, A.; Higgins, S. J.; Nichols, R. J.; Schwarzacher, W., Dual Control of Molecular Conductance through pH and Potential in Single-Molecule Devices. *Nano Lett* **2018,** *18* (2), 1317-1322.

33.   Ai, Y.; Kovalchuk, A.; Qiu, X.; Zhang, Y.; Kumar, S.; Wang, X.; Kühnel, M.; Nørgaard, K.; Chiechi, R. C., In-Place Modulation of Rectification in Tunneling Junctions Comprising Self-Assembled Monolayers. *Nano Lett* **2018,** *18* (12), 7552-7559.

34.   Kumar, S.; Merelli, M.; Danowski, W.; Rudolf, P.; Feringa, B. L.; Chiechi, R. C., Chemical Locking in Molecular Tunneling Junctions Enables Nonvolatile Memory with Large On–Off Ratios. *Adv. Mater.* **2019,** *31*, 1807831.

35.   Zhang, Y.-P.; Chen, L.-C.; Zhang, Z.-Q.; Cao, J.-J.; Tang, C.; Liu, J.; Duan, L.-L.; Huo, Y.; Shao, X.; Hong, W.; Zhang, H.-L., Distinguishing Diketopyrrolopyrrole Isomers in Single-Molecule Junctions via Reversible Stimuli-Responsive Quantum Interference. *J Am Chem Soc* **2018,** *140* (21), 6531-6535.

36.   Rogers, K. S.; Clayton, C. C., Effects of pH on benzimidazole fluorescence. *Analytical Biochemistry* **1972,** *48* (1), 199-201.

37.   Kamplain, J. W.; Bielawski, C. W., Dynamic covalent polymers based upon carbene dimerization. *Chem. Commun.* **2006,** *5* (16), 1727.

38.   Boydston, A. J.; Xia, Y.; Kornfield, J. A.; Gorodetskaya, I. A.; Grubbs, R. H., Cyclic Ruthenium-Alkylidene Catalysts for Ring-Expansion Metathesis Polymerization. *J Am Chem Soc* **2008,** *130* (38), 12775-12782.

39.   Khramov, D. M.; Boydston, A. J.; Bielawski, C. W., Synthesis and Study of Janus Bis(carbene)s and Their Transition-Metal Complexes. *Angew. Chem. Int. Ed.* **2006,** *45* (37), 6186-6189.

40.   Shilova, E. A.; Heynderickx, A.; Siri, O., Bandrowski's Base Revisited: Toward a Unprecedented Class of Quinonediimines or New Two-Way Chromophoric Molecular Switches. *J Org Chem* **2010,** *75* (6), 1855-1861.

41.   Frisch, M. J.; Trucks, G. W.; Schlegel, H. B.; Robb, G.; Cheeseman, J. R.; Montgomery Jr, J. A.; Iyengar, S. S., Gaussian03-Version c01. *Gaussian Inc Wallingford CT* **2004**.

42.   Becke, A. D., Density-functional thermochemistry. III. The role of exact exchange. *The Journal of Chemical Physics* **1993,** *98* (7), 5648-5652.

43.   Farkas, Ö.; Schlegel, H. B., Methods for optimizing large molecules. Part III. An improved algorithm for geometry optimization using direct inversion in the iterative subspace (GDIIS). *Physical Chemistry Chemical Physics* **2002,** *4* (1), 11-15.

44.   Bürgi, R.; Kollman, P. A.; van Gunsteren, W. F., Simulating proteins at constant pH: An approach combining molecular dynamics and Monte Carlo simulation. *Proteins: Structure, Function, and Bioinformatics* **2002,** *47* (4), 469-480.

45.   Ibragimova, G. T.; Wade, R. C., Importance of Explicit Salt Ions for Protein Stability in Molecular Dynamics Simulation. *Biophysical Journal* **1998,** *74* (6), 2906-2911.

46.   Singh, U. C.; Kollman, P. A., A combined ab initio quantum mechanical and molecular mechanical method for carrying out simulations on complex molecular systems: Applications to the CH3Cl + Cl− exchange reaction and gas phase protonation of polyethers. *Journal of Computational Chemistry* **1986,** *7* (6), 718-730.

47.   Soler, J. M.; Artacho, E.; Gale, J. D.; García, A.; Junquera, J.; Ordejón,P.; Sánchez-Portal,D., The SIESTA method for ab-initio order-N materials simulation.*J. Phys.: Condens. Matte*r 2002, *14(11)*, 2745.

48.   Perdew, P.J.; Burke, K.;Ernzerhof, M., Generalized Gradient Approximation Made Simple,*Phys.Rev.Lett.*,1996,*77(18)*,3865-3868.

49.   Ferrer, J.; Lambert, C. J.; Garcia-Suarez, V. M.; Manrique, D. Z.; Visontai, D.; Oroszlany, L. Rodriguez-Ferradas, R.; Grace, I.; Bailey, S. W. D.; Gillemot, K.; Sadeghi, H.; Algharagholy, L. A., GOLLUM: a next-generation simulation tool for electron, thermal and spin transport, *New J.phys*.,2014,*16(9)*,093029.

50.   Smaali, K.; Clement, N.; Patriarche, G.; Vuillaume, D., Conductance Statistics from a Large Array of Sub-10 nm Molecular Junctions. *ACS Nano* **2012,** *6* (6), 4639-4647.

51.   Clement, N.; Patriarche, G.; Smaali, K.; Vaurette, F.; Nishiguchi, K.; Troadec, D.; Fujiwara, A.; Vuillaume, D., Large Array of Sub-10-nm Single-Grain Au Nanodots for use in Nanotechnology. *Small* **2011,** *7* (18), 2607-2613.

52.   Audi, H.; Viero, Y.; Alwhaibi, N.; Chen, Z.; Iazykov, M.; Heynderickx, A.; Xiao, F.; Guerin, D.; Krzeminski, C.; Grace, I.M.; Lambert, C.J.; Siri, O.; Vuillaume, D.; Lenfant, S.; Klein, H., Electrical molecular switch addressed by chemical stimuli. *Nanoscale* 2020,*12*(18), 10127-10139.

Chapter 5

The role of quantum interference in conductance oscillations in folded carbazoles

This study is a collaborative work between (Lancaster, Durham and Madrid Universities). The experiments are still in progress.

5.1. Introduction

In recent years, one topic of interest in the field of charge transport at the molecular-scale has been quantum interference (QI) effects [1,2,3,4,5]. This is because it provides a novel approach to tuning transport behaviour, by enhancing or decreasing the conductance (i.e. constructive or destructive quantum interference) in molecular systems [6]. Such effects can be utilized in the design of single-molecule electronic or thermoelectric [7-8] components to achieve the quantum effects that occur at the nanoscale level. Typically, such behaviour is built into the structure of the molecule, for example through the connectivity of the anchor groups to a central core [9,10,11], however the ideal case would be to control the interference features through an external mechanism. One typical approach to this is through mechanical control, where the structure of the molecule can be changed to alter the interference pattern [12]. Other types of molecular structures that have shown excellent potential in controlling quantum interference is the stacking of individual molecules[7,13,14]. Here the electrodes attached to one anchor at the end of two molecules, which stack to form a dimer. Moreover, this will bridge the gap between the electrodes and the electron path between them will be via the overlap π -orbitals of the molecules overlap. Here controlling the nature of the overlap has shown conductance oscillations as destructive interference features are sensitive to the stacking geometry. Understanding the charge transfer through π-stacked assemblies plays an important role in designing and development the electronic devices.

The present research aims to explore experimentally and theoretically, the correlation between pi-stacking and controlling the quantum interference in a series of pi-stacked Carbazole molecules FC1, FC2 and FC3 as shown figure 5.1. Typically to create pi-stacked junctions, molecules with a single anchor group are used, as they should only bind to one electrode and therefore to create a molecular bridge across the junction two molecules will have to stack as shown in Figure 5.2. However, the junction formation probability is an unknown quantity using this approach, therefore to create a stacked geometry, it is useful to join the two molecules together via a tether to their central core, as shown in figure 5.1. FC1 is a para connected monomer with a single thiol anchor group, formed of a carbazole core unit with an alkane chain attached to the central nitrogen atom. FC2 is the dimer consisting of two FC1 molecules now connected (tethered) via the connecting alkane chain. FC3 consists of a different tether unit, which is now a more rigid phenyl ring with tertiary butyl group. The aim is to control the stacking geometry via the tether unit, which in the case of FC3 should increase the distance between the carbazole units. The choice of the thiol anchoring groups ensures a strong chemical bonding to the leads with the current flow mainly controlled by the molecular HOMO level[15-17].
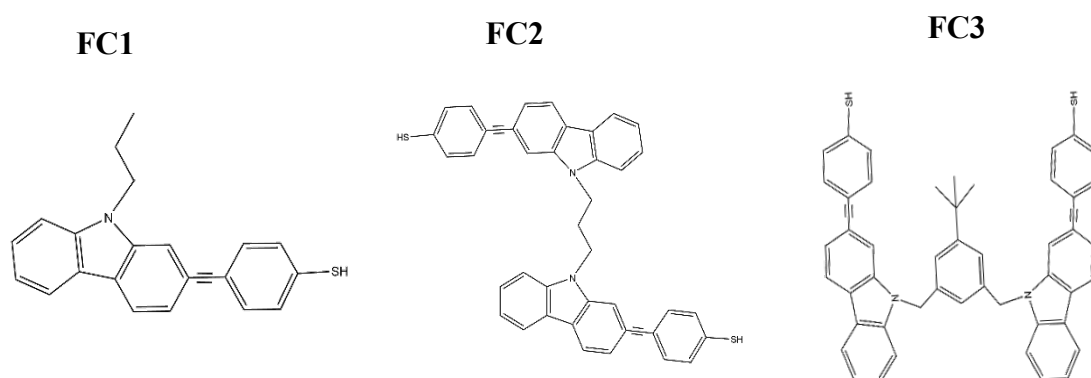
Figure 5.1: The molecular structures used in this study : (FC1) a single carbazole with one thiol anchor group, (FC2) two carbazole with thiol anchor groups tethered by alkane chain, and (FC3) have two carbazoles with thiol anchor groups tethered by a longer tether with a phenyl ring in it.

The conductance of these molecules was measured in Madrid using a scanning tunneling microscope - break junction (STM-BJ) technique[6,13]. In this technique, a metallic contact between a gold STM tip and a gold coated substrate is created with the use of a piezoelectric actuator. The conductance across this junction is measured continuously as the metal contact is ruptured by retracting the tip. This process is repeated thousands of times generating conductance versus displacement traces each of which is an independent measurement (Magyarkuti, A., Adak, O., Halbritter, A., & Venkataraman, L)[18]. Table 1   shows the experimental conductance and each molecule has three different conductance values. This suggest that there are multiple junction geometries are being formed, and surprisingly the same behaviour is seen in the monomer (FC1) as for the dimer systems (FC2 and FC3). The value of the high, middle and low conductance values is also similar in each case and follow the same trend. To aid the attribution of the conductance values, I will investigate different possible geometries binding in different places for these three molecules. Thus, using DFT and transport calculations will provide insight into what may be happening in the experimental data and how these molecules behave in the junction.

Table 1. The experimental conductance measurements for the all three molecules FC1, FC2 and FC3. Each molecule shows three conductance values determined from their conductance histograms. (Unpublished data, provided by Juan Hurtado, Universidad Autónoma de Madrid)

	Log G_h (G_0)	Log G_m (G_0)	Log G_l (G_0)
FC1	-2.8	-4	-5.2
FC2	-2.85	-4.7	-5.2
FC3	-3.1	-3.95	-4.9

5.2. Theoretical Methods

5.2.1 Molecules in the gas phase

The first step in modelling the electronic properties is to calculate optimum geometry of the three molecules. Examining the structure of the tethered molecules FC2 and 3, I identify 3 possible geometries that they could form. These are shown in Figure 5.2 and consist of the non-stacked or 'open' configuration (a), a 'half-stacked' geometry where the thiol anchor groups lie at opposite ends and only the core carbazole unit is stacked (b), and the fully stacked or 'hairpin' geometry where the anchor groups lie on the same side (c). I then relax the FC1 molecule and the FC2 and FC3 for the three different configurations using the DFT method employed to calculate the optimum configurations. This was done using the density functional SIESTA code [19], by relaxing them to force tolerance less than 0.02eV/Å using a double-zeta basis set, and a real- space grid defined with an energy cutoff of 150 Rydberg. The exchange-correlation functional was the Van der Waals functional [20] which more accurately describes the longer-range interactions in the stacked junctions. I also repeat the calculations using the Local Density Approximation (LDA) [21] to compare the accuracy of different functionals.
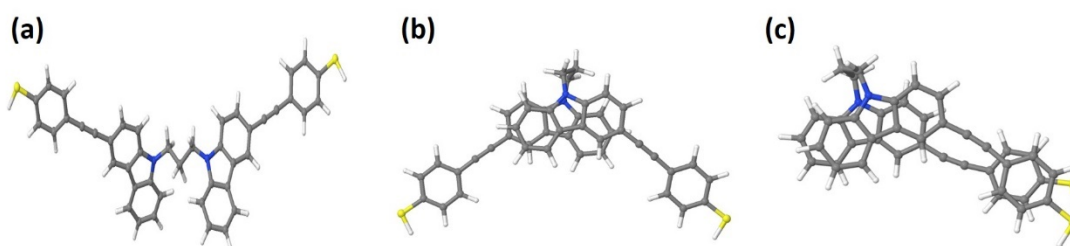
Figure 5.2 Three possible configurations of the FC2 molecule: (a) the 'open' non folded geometry, (b) 'half-stacked' where the anchor groups lie at opposite ends and (c) 'hairpin' where the anchor groups are at the same end.

94

Table 2 shows the minimum ground state energy for each of the three configurations using a VdW functional. In the case of FC1, the open case is for the dimer structure in a non-stacked configuration. In each case the highest energy occurs for the 'open' (non-stacked) geometry and I set this value to 0eV. The energy of the other configurations is then given relative to this value. The energy of the 'hairpin configuration is the lowest in all configurations, i.e. for FC1 it is -2.5eV compared to -1.8 eV for the 'half-stacked' and FC3 is -1.4eV (hairpin) compared to -0.8eV (half-stacked).

The same behaviour is found using the LDA functional (Table 3). These results demonstrate which conformations are the most favorable to be measured or formed in the junction, as I compare the number difference with Boltzmann factor where $k_B T =$ 0.0259 eV at room temperature T. The energy differences between the structures are much greater than $k_B T$ and suggest that the most likely structure for the tethered molecule FC2 and FC3 to be present in the junction is the hairpin configuration. As a first step to evaluating the experimental behaviour, this may explain why all three molecules produce similar conductance groups, as they all have anchor groups on one side of the molecule in the lowest energy geometry.

Table 2 Ground state energy for the optimum geometry of molecules FC1 (dimer), FC2 and FC3 calculated using VdW.

structure / molecule	open	Hairpin	Half-stacked
FC1	0 eV	-2.5 eV	-1.8 eV
FC2	0 eV	-1.34 eV	- 0.78 eV
FC3	0 eV	-1.4 eV	-0.8 eV

Table 3 Ground state energy for the optimum geometry of molecules FC1 (dimer), FC2 and FC3 calculated using LDA.

Structure / molecule	Open	Hairpin	Half stacked
FC1	0 eV	-2.2 eV	-1.5 eV
FC2	0 eV	-1.01 eV	-0.5 eV
FC3	0 eV	-0.8 eV	-0.7 eV

Each of the molecules has a lower energy in the stacked geometry compared to the open configuration, which suggests that the binding energy between the carbazoles is large. I evaluate the strength of the binding energy for FC1 by calculating it as a function of the stacking parameters defined in Figure 5.4 (X is the overlap length of the molecules and d is separation between them). Figure 5.3Shows the binding energy

has a minimum value of -0.5eV (X=6 Å and d=3.6Å) for the half-stack and -0.33eV (X=6.2 Å and d=3.4 Å)where X is the overlap length of the molecules and d is separation between them. This energy is large and is comparable to the typical binding energies between anchor groups and gold electrodes.
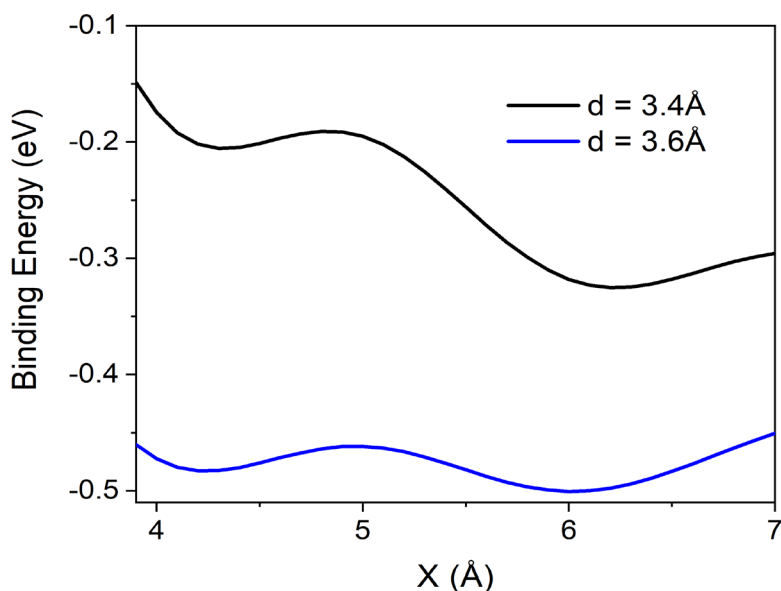
Figure 5.3 Binding energy between two FC1 molecules in the half-stack geometry (Figure 5.4) as a function of overlap length X for two different molecule separations d.

5.2.2 Binding energy to gold electrodes

The next step is to understand how the molecules FC1, FC2 and FC3 attach to the surface of the gold electrodes and in this case as I am modelling STM-Break junction measurements, I assume that the gold surface consists of a pyramid of gold atoms. I then calculate the optimum binding geometry of each molecule. For these molecules, the expected binding is through the tip of the gold coupling to the terminal sulfur atom in each molecule. The binding distance d_b defined as the distance between the gold - sulfur. The ground state energy of the total structure (E_{AB}^{AB}) calculated using SIESTA,

with the parameters defined as those in section (5.2.1). In SIESTA, I calculate the energy of each monomer in a fixed basis. Thus, the energy of the individual molecule in the presence of the fixed basis well-defined as E_A^{AB} and for the electrode is E_B^{AB}. To calculate the binding energy, I will use the following equation:

$$\Delta E(AB) = E_{AB}^{AB} - E_A^{AB} - E_B^{AB}$$

The optimum binding distance d_b between Au-S is 2.3 Å, and the binding energy is approximately -1.9 eV. In the case of FC1, with one anchor group, it would be expected that the only possible geometry to bridge the junction is in the half-stacked configuration. However, the measured values in Table 4 show three groups, suggesting that the molecule may be binding to the gold through other parts of the molecule rather that the sulfur atom of the thiol anchor. Therefore, I consider the binding energy for the three molecules FC1, FC2 and FC3 in three different positions which are: (i) connecting through the terminal hydrogen, (ii) connecting through the Nitrogen in the central core of the Carbazole and (iii) the cofacial arrangement binding to the terminal phenyl group. These geometries are shown in Tables: 4 (FC1), 5 for (FC2) and (FC3). What I find is that all of them give binding energies much larger than room temperature, but the values (typically ~0.15 eV) are slightly less than the Au-S bond and the stacking binding energy. Also, the binding energy is the largest when it is connecting through the terminal hydrogen as presented in Table 4(b, e) and Table 5 (b). The binding to the terminal hydrogen could be due to interaction with the pi-system of the molecule, which may be stronger at the ends of the molecule where there is less chance of repulsion due to alkane chains near the central region. Therefore, it could be possible that the molecules bridge the junctions in these geometries.

Table 4. Binding energy and binding distance for FC1 connected to the electrode (a)through H (b) in cofacial through H (c) in co-facial through N, and binding energy for pi-stacked carbazole in HAIRPIN structures connected to the electrode (d)through H (e) in cofacial through H (f) in cofacial through N.
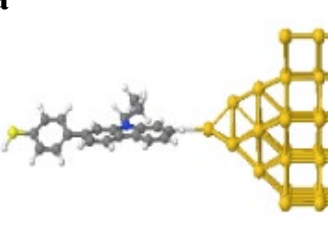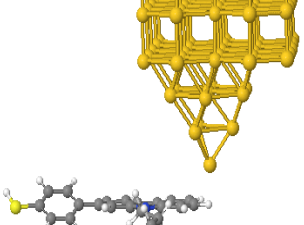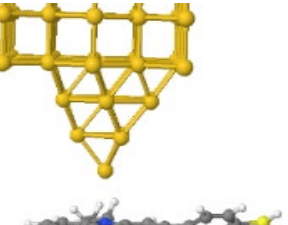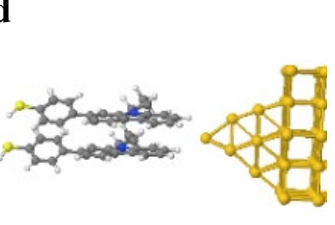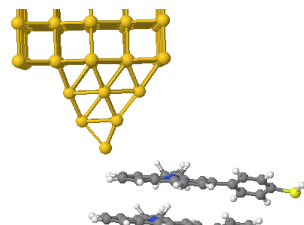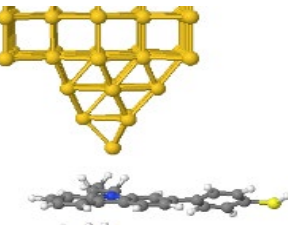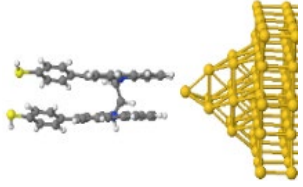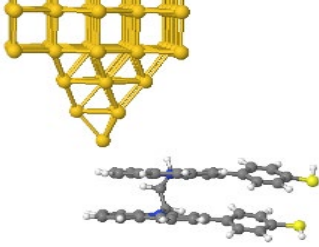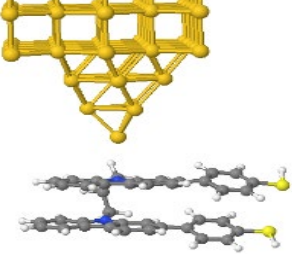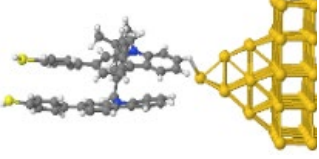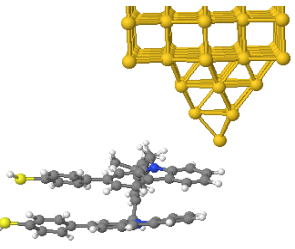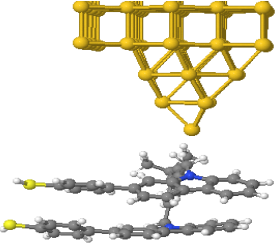
	FC1: Single carbazole		
structure	a	b	c
Binding energy	-0.13 eV	-0.17 eV	-0.11eV
Binding distance	2.1 A°	2.3 A°	3 A°
	Pi-stacked FC1		
structure	d	e	f
Binding energy	-0.16 eV	-0.18 eV	-0.11eV
Binding distance	H1: 2.5 A° H2: 2.7 A°	2.3 A°	3.3A°

Table 5. The binding energy and binding distance for the molecules FC2 and FC3 in hairpin structures connected to the gold (a)through H (b) in cofacial through H (c) in cofacial through N.

	FC2		
structure	a	b	c
Binding energy	-0.15eV	-0.17 eV	-0.12 eV
Binding distance	H1:2.2 A° H2: 2.9A°	2.3 A°	3.1 A°
	FC3		
structure	a	b	c
Binding energy	-0.14 eV	-0.16 eV	-0.05 eV
Binding distance	H1: 2.3 A° H2: 2.7A°	2.3 A°	3.5 A°

5.2.3 Metal/Molecule/Metal junction:

I now explore the electron transport properties of the carbazole molecules shown for all the possible geometries that were previously considered, and the different electrode binding locations. In each case, an extended molecule is constructed, with the electrodes consisting of 5 layers of (111) gold each containing 25 atoms terminated by a pyramid of 11 gold atoms. SIESTA is then used to generate a Hamiltonian using the parameters described previously (here an LDA functional is used to minimize computational expense as the transport properties are not strongly dependent on the functional). The zero-bias transmission coefficient $T(E)$ is calculated using this Hamiltonian, via the GOLLUM code [22,23]. The room temperature conductance can then evaluate from the Landauer formula,

$$G = \frac{2e^2}{h} \int_{-\infty}^{\infty} dE \, T(E) \left(\frac{df(E)}{dE} \right)$$

where $f(E)$ is the Fermi-Dirac distribution, e is the electronic charge and h is Planck's constant.

5.3. Results and discussion

In the following sections, I will present different binding locations on the gold electrode for the folded carbazoles FC1, FC2 and FC3 with the corresponding conductance values. Also, I will investigate which molecules show quantum

interference effects, namely a DQI (destructive quantum interference) feature and how it is controlled by the stacking geometry.

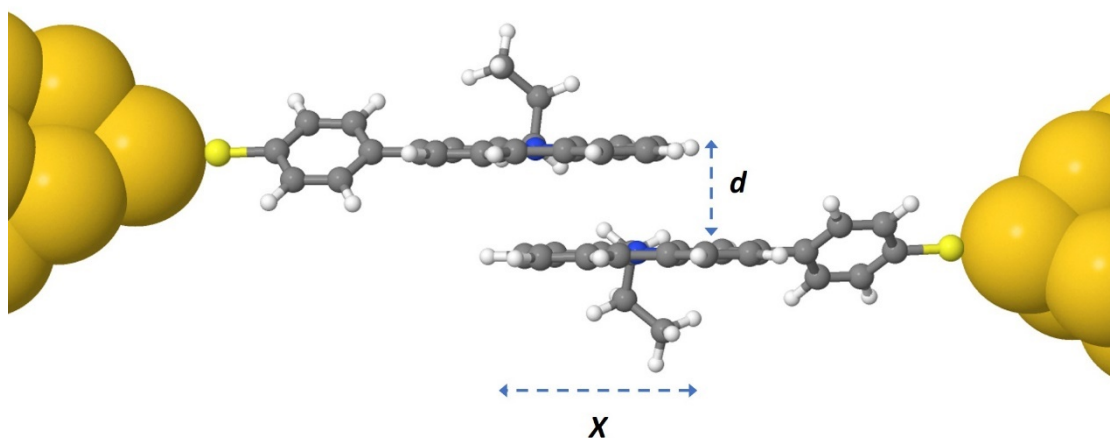## 5.3.1 Transmission coefficients

5.3.1.1. FC1:

Figure. 5.4 Geometry of FC1 in a pi-stacking geometry. X is the overlap length of the two molecules and d is the separation**.**

As a first step, I examine the transport behaviour of FC1 when it forms a half-stacked geometry to compare it to previous work [7,13,14] on these types of structures. The molecule bridges the junction by forming the structure shown in Figure 5.4 with the parameters d and X defining the geometry, d is the separation between the stacked layers and X is the overlap length of the molecules. In the case of the two molecules being perfectly aligned on top of one another the value of X would equal the length of the molecule. The optimum binding distance was found to be d_b=3.6Å and I calculate

the transmission coefficient $T(E)$ for different overlap length ranging from X=3.9 to 7.9Å (Figure 5.5). The results show how the transport is sensitive to the overlap length, with DQI features appearing at values of X=4.9 and 6.9Å. I then evaluate the conductance at a Fermi energy $E_F^1 = E_F^0 + 0.5eV$ (where E_F^0 is the DFT predicted Fermi energy), which avoids the pinning to the HOMO resonance caused by the thiol anchor groups [15-17]. Here, the conductance oscillates with X, varying by over 2 orders of magnitude. This shows that carbazoles behave in a similar way to previously studied systems and quantum interference features can be controlled over a small change of geometry (approx. 1Å).
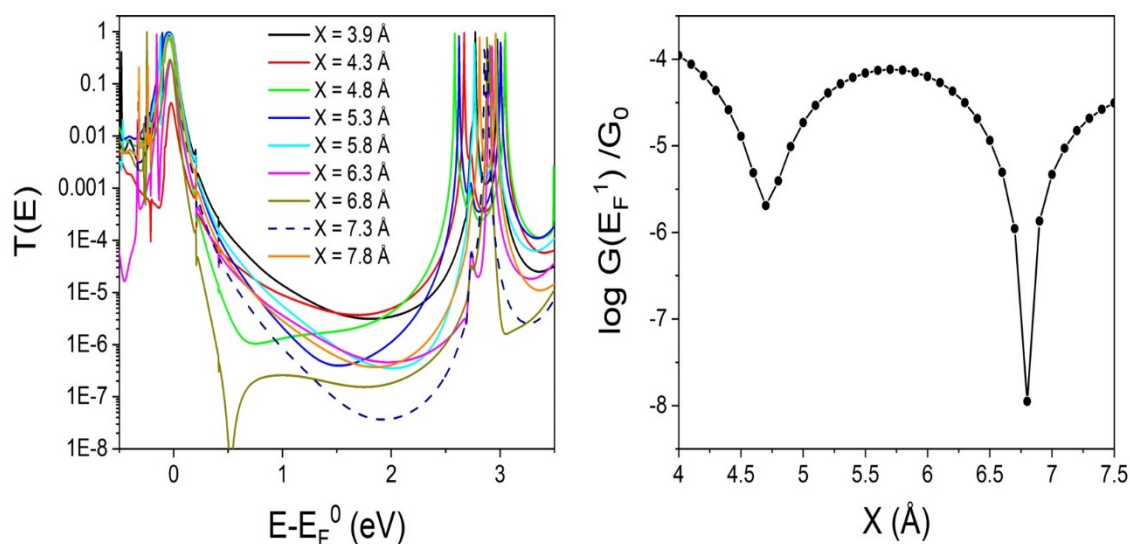

Figure 5.5 (Left) Zero-bias transmission coefficient T(E) and conductance G (right) of molecule FC1 half-stacked geometry defined in Figure 5.4 For different values of X at a separation d=3.6Å.

As shown in the optimum geometry calculations, the half-stacked dimer configuration for FC1 isn't the most favourable, therefore I explore all possible bridging geometries for both the monomer and dimer using the binding locations calculation in section (5.2.2).   Figure 5.6 (**A**) shows the transmission through the single carbazole

unit FC1 for three different binding geometries, where the DFT predicted fermi energy corresponding to (E_F -E_F^{DFT} =0 eV) lies close to the HOMO resonance. The first configuration (**1** blue), for one thiol anchor group attached to the gold on one side, and the terminal hydrogen atom on the carbazole attached to the gold as another anchor group shows the lowest transmission value. The second geometry (**2** red) considers the co-facial binding connecting to the central core of the carbazole molecule to one electrode, as the thiol is connected to the second. This geometry has the highest transmission value $T(E)$ in the HOMO-LUMO gap. The last geometry (**3** gold) for the co-facial binding through the terminal phenyl ring gives a value of T between the two previous geometries. Therefore, for the single molecule junction, where the second electrode is weakly coupled, the value of the transmission is controlled by the coupling strength between electrode and the pi-system of the molecule.
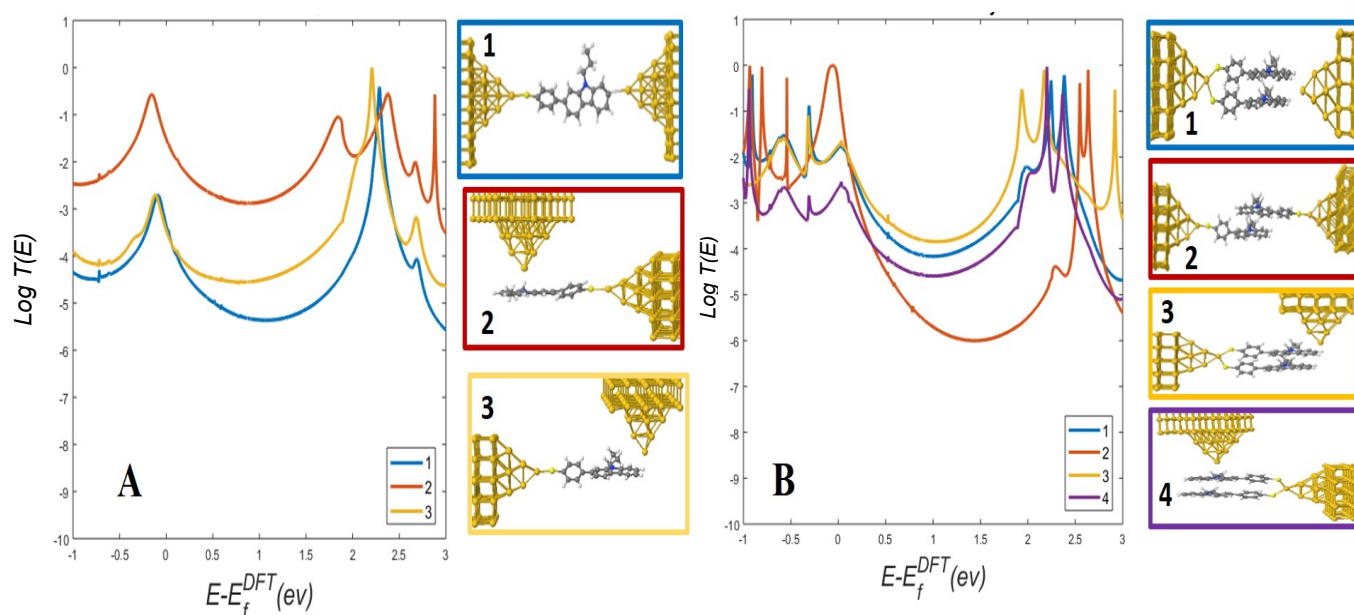

Figure5.6: The transmission coefficient T(E) of different bridging geometries for the FC1 monomer (**A**) and the FC1 stacked dimer (**B**).

Next, I investigate the bridging geometry of FC1 for the dimer stacked configurations and the results are shown in Figure 5.6 (**B**). The first structure is the fully

stacked or hairpin, where the two sulfurs are at the same end (**1** blue) and the two terminal hydrogens bind to the second electrode. The second case is the half stacked, where the sulfur atoms are at the opposite end (**2** red) as was the case calculated in Figure 5.5. For the optimum configuration there is no DQI feature in the gap. The hairpin geometry binding through the pi-system (cofacial) of the terminal phenyl ring (**3** gold) and central core (**4** blue) are also shown. I observe that the hairpin configuration has the higher conductance values, and the half stacked is the lowest. In all the stacked geometries there are no destructive interference resonances (DQI) in the gap between the HOMO and LUMO resonances. All three hairpin configurations give similar conductance value as in this case the terminal hydrogens now couple twice to the gold increasing the coupling strength.

The experimental measurements of FC1 show three conductance values, and I have identified different bridging geometries FC1 could form. Theoretically, the high conductance value occurs when a single molecule binds with a strong co-facial coupling, the middle value occurs for the hairpin geometry and the low conductance is given by the half-stacked configuration.

5.3.1.2. FC2 & FC3:

Having studied FC1, I will now move on to discuss the different binding locations of the folded carbazoles FC2 and FC3 and their electrical transports curves. The results for FC2 are shown in Figure 5.7, the first geometry (**1** blue) is the hairpin configuration where one of the electrodes contacts the terminal hydrogen atoms, and the other is coupled to the terminals sulfur. The second structure is the Half-stacked, where the gold binds to the sulfur atom at the opposite ends (**2** red). Also, I investigate the hairpin

model when the gold electrode is connecting in co-facial form through two different sites, which are the terminal phenyl ring (3 gold) and the core of the carbazole molecule (**4** purple). The last structure is the open system for the unfolded carbazole, where the electrode connected to the terminal sulfur at both ends, but the central core is not stacked (**5** green).
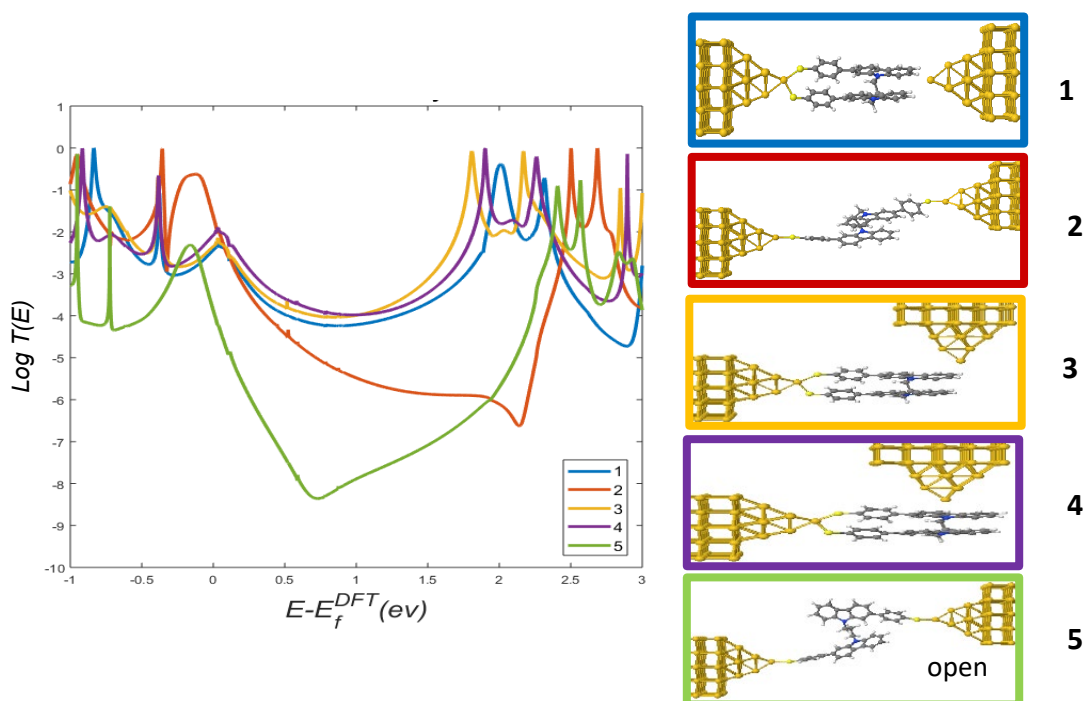

Figure 5.7: The transmission coefficient T(E) for different bridging geometries of the FC2 molecule.

In Figures 5.7 there is a clear trend in the transmission curves; the gold, purple and blue lines have the highest transmission values in the gap and all show similar behaviour. They correspond to the three different bridging geometries of the hairpin configuration. In this case the binding through two terminal hydrogen atoms now gives a coupling strength similar to the co-facial geometries. The half-stacked geometry (red)

shows a lower transmission and a DQI feature which is well away from the Fermi energy (0eV), in this case the tether of FC2 fixes the stacking overlap at a position where the DQI occurs in the gap. Finally, the lowest transmission occurs for the open geometry which also shows destructive interference in the gap. Therefore, for FC2, the results show three clear conductance values, a high conductance for the hairpin, middle value for the half-stacked and low for the open.
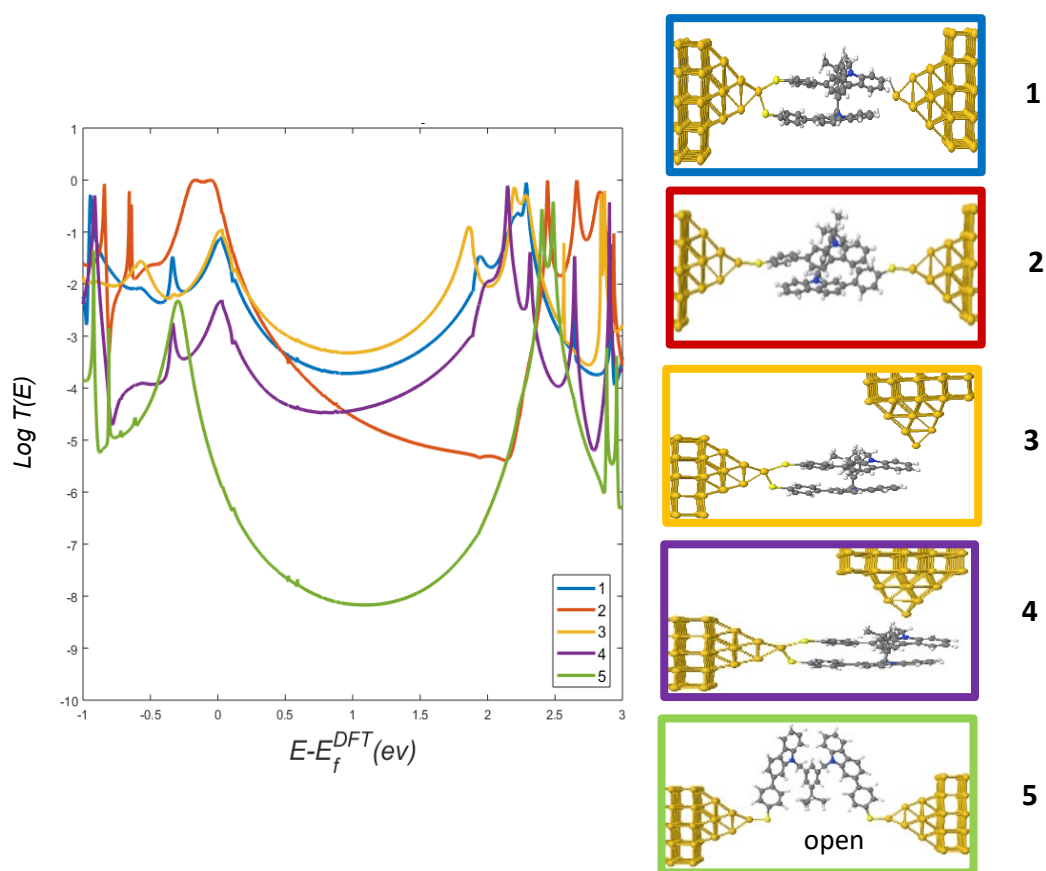

Figure 5.8. The transmission coefficient of FC3 for different bridging geometries.

The equivalent bridging geometries are then calculated for the FC3 molecule and the results are shown in Figure 5.8 The results follow the same pattern as FC2, with the hairpin geometry having the highest transmission value in the HOMO-LUMO gap,

followed by the half-stacked and the lowest is given by the open. The main difference is the different binding geometries of the hairpin gives a wider range of conductance values. The half stacked geometry again shows a DQI feature at a similar position close to the LUMO resonance, which suggests that the nature of the tether doesn't affect the quantum interference and only the stacking geometry which it controls is important.

In summary, these two tethered molecules have three stacking configurations, which could explain the conductance groups. However, the gas phase calculations suggest that the hairpin geometry is the most energetically favourable. While it is possible that the invasive break junction approach could lead to the higher energy configurations occurring, it seems likely that the hairpin geometry is responsible and, in this case, follows the behaviour of the FC1 monomer. One clear difference between the hairpin and the other two (half-stacked and open) is that it doesn't show destructive quantum interference, therefore mechanical manipulation of the junction (i.e. by extending and closing the junction), shouldn't show large conductance oscillations as predicted in Figure 5.4.

5.3.2 Sliding contacts along the gold electrodes for FC2 and FC3

Control of the stacking geometry through the separation between the gold-electrodes only occurs when the molecular junction is fully extended. I now investigate the behaviour of the molecules for smaller lead separations, i.e. when the molecules slide along the surface of the electrodes. I investigate two situations comparing the behaviour of the half-stacked FC2 molecule with the open FC3 molecule. These are chosen for simplicity as they have thiol anchors on opposite sides, so it is easier to control the sliding geometry and one (FC2) shows destructive quantum interference while the other (FC3) does not.

Figure 5.9 shows the different positions (1-4) of the FC2 molecule as it slides across the tip of the gold electrodes. The transmission shows that for different contact separations the resonances shift as well as the DQI feature. Figure (5.9a) shows the evaluated conductance at the Fermi energy as a function of the electrode separation X and shows that it oscillates. Also, it shows a counterintuitive behaviour, in that the conductance is highest for the largest contact distance X. There are multiple positions that the molecule could take as it slides along the surface, Figure (5.9 b and c) repeat the calculation for different sliding geometries and show similar behaviour to a, only the nature of the oscillations change.
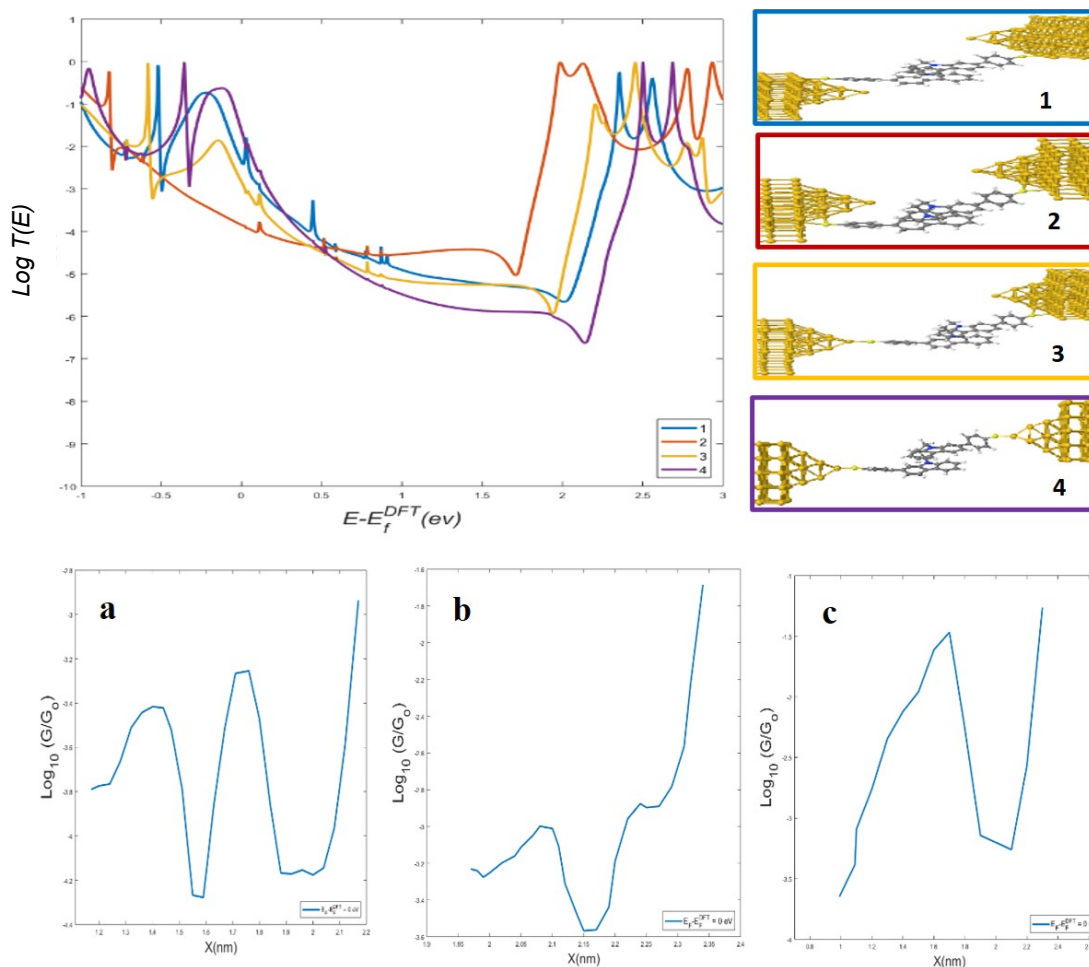
Figure 5.9 (top) Transmission coefficient T(E) of molecule FC2 (half-stacked) for four different geometries (1-4) controlled by the contact separation X between the electrode. (bottom a-c) Conductance as a function of X for three different starting configurations.

I then repeat the calculation for the open FC3 molecule (Figure 5.10). Here the molecule has no DQI feature and the transmission in the gap simply decreases as the contact separation is increased. This leads to the case (a and c) where the conductance is lowest for the largest separation X.
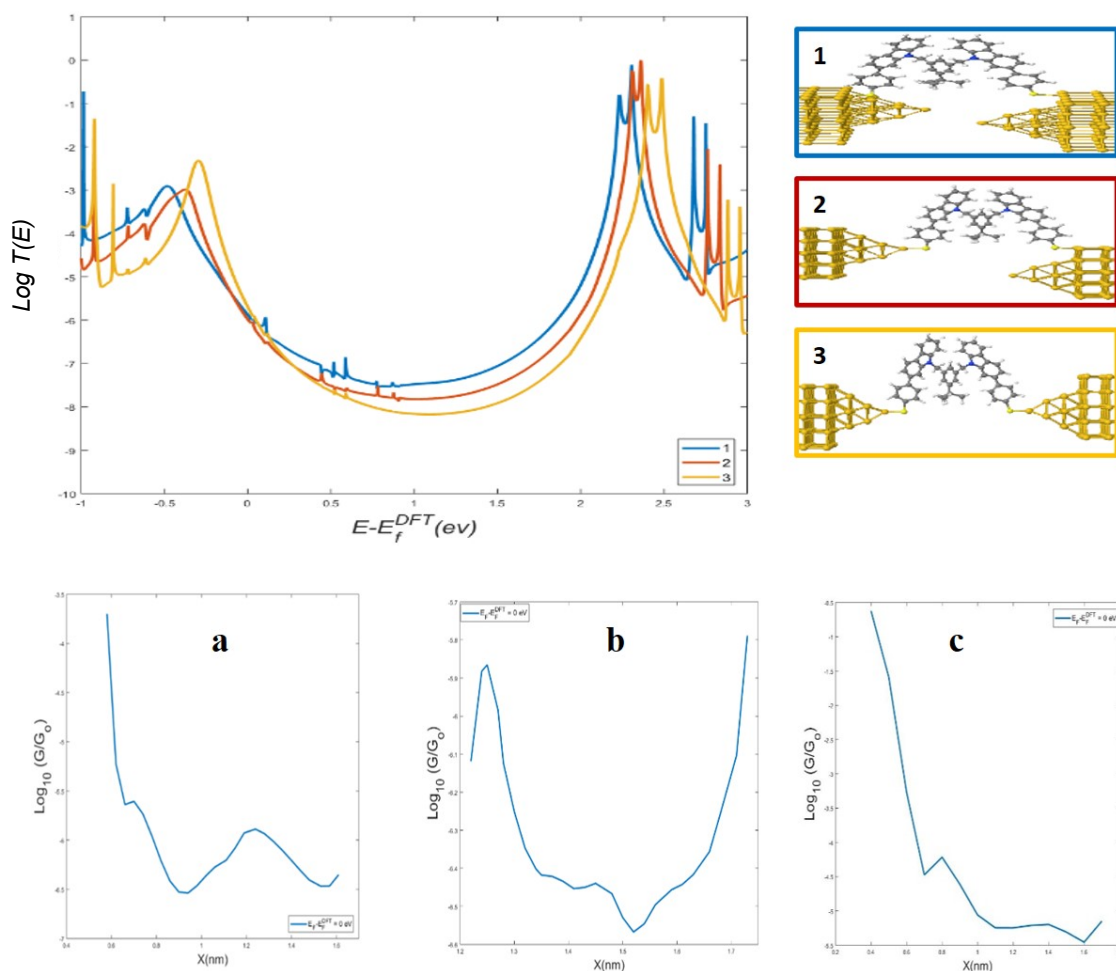
Figure 5.10. (top) Transmission coefficient T(E) of molecule FC3 (open) for four different geometries (1-4) controlled by the contact separation X between the electrode. (bottom a-c) Conductance as a function of X for three different starting configurations.

5.4. Conclusion

Folded carbazoles where designed to control the formation of pi-stacking bridges in molecular junctions. Experimental measurements of the conductances of these molecules show three conductance groups for both the monomer and folded forms. I have carried out a theoretical study based on DFT calculations to explain these results and have explored the possible conformations that the FC1, FC2, and FC3 molecules can form in a junction. Using a highly accurate VdW functional to describe the

interactions between stacked molecules, I find that the binding energy between carbazoles is quite large (~0.5eV) and the most favourable configuration is the hairpin geometry. I have computed the transmission coefficients and the conductance in different bridging geometries for the three molecules, which are the monomer form, unfolded (open) system, and the stacked molecule (i.e. hairpin and half-stacked). The DFT results show the conductance is highest for the hairpin configuration, which does not show any destructive quantum interference, the middle value is the half-stacked which does show DQI and the low conductance occurs in the non-folded open geometry. I have also investigated multiple binding locations to show that the monomer or hairpin form can contact to the second electrode via the terminating hydrogens or through the pi-system in a co-facial binding geometry.

To explore the role of quantum interference in folded carbazoles molecules, I have investigated changing the electrode separation which can control the overlap length of the molecule, in FC1 this leads to conductance oscillations as the DQI feature moves in and out of the HOMO-LUMO gap. At shorter electrode separations, varying the separation can cause the molecule to 'slide' along the electrode. This behaviour also shows oscillations in the conductance, but in the case where a DQI feature occurs the conductance tends to increase with separation while in systems with constructive interference the conductance decreases.

Bibliography

[1] Baer, R. and Neuhauser, D. (2002). Phase coherent electronics: A molecular switch based on quantum interference. *Journal of the American Chemical Society*, *124*(16), 4200–4201. https://doi.org/10.1021/ja016605s

[2] Cardamone, D. M., Stafford, C. A., & Mazumdar, S. (2006). Controlling quantum transport through a single molecule. *Nano Letters*, *6*(11), 2422–2426. https://doi.org/10.1021/nl0608442

 [3] Guédon, C. M., Valkenier, H., Markussen, T., Thygesen, K. S., Hummelen, J. C. and Van Der Molen, S. J. (2012). Observation of quantum interference in molecular charge transport. *Nature Nanotechnology*, *7*(5), 305–309. https://doi.org/10.1038/nnano.2012.37

[4] Lambert, C. J. (2015). Basic concepts of quantum interference and electron transport in single-molecule electronics. *Chemical Society Reviews*, *44*(4), 875–888. https://doi.org/10.1039/c4cs00203b

[5] Su, T. A., Neupane, M., Steigerwald, M. L., Venkataraman, L. and Nuckolls, C. (2016). Chemical principles of single-molecule electronics. *Nature Reviews Materials*, *1*. https://doi.org/10.1038/natrevmats.2016.2

[6] Liu, J., Huang, X., Wang, F. and Hong, W. (2019). Quantum Interference Effects in Charge Transport through Single-Molecule Junctions: Detection, Manipulation, and Application. *Accounts of Chemical Research*, *52*(1), 151–160. https://doi.org/10.1021/acs.accounts.8b00429

[7] Kiršanskas, G., Li, Q., Flensberg, K., Solomon, G. C. and Leijnse, M. (2014). Designing π-stacked molecular structures to control heat transport through molecular junctions. *Applied Physics Letters*, *105*(23). https://doi.org/10.1063/1.4903340

[8] Li, Q. and Solomon, G. C. (2014). Exploring coherent transport through π-stacked systems for molecular electronic devices. *Faraday Discussions*, *174*, 21–35. https://doi.org/10.1039/c4fd00083h

[9] Geng, Y., Sangtarash, S., Huang, C., Sadeghi, H., Fu, Y.; Hong, W.; Wandlowski, T., Decurtins, S., Lambert, C.J. and Liu, S.X., (2015)., Magic ratios for connectivity-driven electrical conductance of graphene-like molecules. *Journal of the American Chemical Society*, *137*(13), 4469-4476.

[10] Gantenbein, M., Wang, L., Al-Jobory, A. A., Ismael, A. K., Lambert, C. J., Hong, W., & Bryce, M. R. (2017). Quantum interference and heteroaromaticity of para- and meta-linked bridged biphenyl units in single molecular conductance measurements. *Scientific reports*, *7*(1), 1-9.

[11] Miao, R., Xu, H., Skripnik, M., Cui, L., Wang, K., Pedersen, K. G., Leijnse, M., Pauly, F., Warnmark, K., Meyhofer, E. and Reddy, P., (2018). Influence of quantum interference on the thermoelectric properties of molecular junctions. *Nano letters*, *18*(9), 5666-5672.

[12] Stefani, D., Weiland, K. J., Skripnik, M., Hsu, C., Perrin, M. L., Mayor, M., Pauly, F. and Van Der Zant, H.S., (2018). Large conductance variations in a mechanosensitive single-molecule junction. *Nano letters*, *18*(9), 5981-5988.

[13] Martín, S., Grace, I., Bryce, M. R., Wang, C., Jitchati, R., Batsanov, A. S., Higgins, S.J., Lambert, C.J. and Nichols, R.J., (2010). Identifying diversity in nanoscale electrical break junctions. *Journal of the American Chemical Society*, *132*(26), 9157–9164.

[14] Frisenda, R., Janssen, V. A. E. C., Grozema, F. C., Van Der Zant, H. S. J. and Renaud, N. (2016). Mechanically controlled quantum interference in individual Ï-stacked dimers. *Nature Chemistry*, *8*(12), 1099–1104. https://doi.org/10.1038/nchem.2588

[15] Mishchenko, A., Vonlanthen, D., Meded, V., Bürkle, M., Li, C., Pobelov, I. V., Bagrets, A., Viljas, J.K., Pauly, F., Evers, F. and Mayor, M., (2010). Influence of conformation on conductance of biphenyl-dithiol single-molecule contacts. *Nano Letters*, *10*(1), 156–163. https://doi.org/10.1021/nl903084b

[16] Pauly, F., Viljas, J. K., Cuevas, J. C. and Schön, G. (2008). Density-functional study of tilt-angle and temperature-dependent conductance in biphenyl dithiol single-molecule junctions. *Physical Review B - Condensed Matter and Materials Physics*, *77*(15), 1–9. https://doi.org/10.1103/PhysRevB.77.155312

[17] Chen, F., Li, X., Hihath, J., Huang, Z. and Tao, N. (2006). Effect of anchoring groups on single-molecule conductance: Comparative study of thiol-, amine-, and carboxylic-acid-terminated molecules. *Journal of the American Chemical Society*, *128*(49), 15874–15881. https://doi.org/10.1021/ja065864k

[18] Magyarkuti, A., Adak, O., Halbritter, A. and Venkataraman, L. (2018). Electronic and mechanical characteristics of stacked dimer molecular junctions. *Nanoscale*, *10*(7), 3362–3368.

[19] Soler, J. M., Artacho, E., Gale, J. D., García, A., Junquera, J., Ordejón, P. and Sánchez-Portal, D. (2002). The SIESTA method for ab initio order-N materials simulation. *Journal of Physics Condensed Matter*, *14*(11), 2745–2779. https://doi.org/10.1088/0953-8984/14/11/302

[20] Cooper, V. R. (2010). Van der Waals density functional: An appropriate exchange functional. *Physical Review B*, *81*(16), 161104.

[21] Langreth, D. C., & Perdew, J. P. (1977). Exchange-correlation energy of a metallic surface: Wave-vector analysis. *Physical Review B*, *15(6)*), 2884.

[22] Ferrer, J., Lambert, C. J., García-Suárez, V. M., Manrique, D. Z., Visontai, D., Oroszlany, L., Rodríguez-Ferradás, R., Grace, I., Bailey, S.W.D., Gillemot, K. , Sadeghi, H. and Algharagholy, L. A. (2014). GOLLUM: A next-generation simulation tool for electron, thermal and spin transport. *New Journal of Physics*, *16*, 1–37. https://doi.org/10.1088/1367-2630/16/9/093029

[23] Gollum, U. (2014). Gollum 1.0 - User Manual, (June), 1–4.

[24] Lambert, C. J. and Liu, S. X. (2018). A Magic Ratio Rule for Beginners: A Chemist's Guide to Quantum Interference in Molecules. *Chemistry - A European Journal*, *24*(17), 4193–4201. https://doi.org/10.1002/chem.201704488

Chapter 6

Conclusions and Future works

This thesis I investigated theoretically a transport properties at the nano-scale using DFT to obtain insight into electronic structures various molecular devices. I employed a combination of the Landauer method and Green's function theory to study electron transport through molecular junctions, as discussed in chapters 2 and 3, respectively. In the fourth chapter, I introduced a design technique to switch the conductance in a single molecule. This method shows that chemical modification of benzo-imidazole derivatives by substituting the protonated H atom can enhance the electronic conductance or yeld the opposite effect by adding the appropriate side branches like amino-phenyl groups. This effect was also measured experimentally in a self-assembled monolayer (SAM). Therefore, in the future I could expand the theoretical calculations used in this strategy to model a SAM of molecules placed

between gold electrodes. I could also perform more calculations using DFT and compare the conductance of SAM devices made of benzo-(bis)imidazole with various degrees of constructive quantum interference by changing the lateral configurations functional groups. As the single-molecule can significantly describe the self-assembled monolayers' efficiency, I hope that the theoretical model of SAM can capture the generic features of the single-molecule arising from switching the conductance by protonation and get a closer agreement with the experimental results. The main result of the theoretical model was that the alignment of the Fermi level with the HOMO resonance explained the behavior upon protonation. This could be tested by using anchor groups which lead to a different alignment of the Fermi energy, i.e., replacing the thiol groups with pyridine or SME anchors which are more LUMO dominated. This could have important consequences for thermoelectric properties, because the sign of the Seebeck coefficient could be controlled through protonation. It would also be interesting to explore the effect of using alternative electrode materials for molecular electronics, such as graphene [1] or superconducting electrodes [2][3] and provides a great experimental and theoretical platform for future.

Chapter 5 examined the pi-stacked electron transport through folded carbazoles and showed how this model can control the electronic conductance's and quantum interference. The multiple bridging geometries that these structures can take opens up a degree of complexity, which makes it difficult to attribute different bridging geometries to the measured conductance values. This project has thrown up many questions in need of further investigation, such as the thermoelectric properties of π - stacked molecules, which can be achieved by calculating the Seebeck coefficient(S). Enhancing the Seebeck coefficient plays an essential role in developing molecular materials with high thermoelectric efficiency[4-5]. It would be interesting to see how

these systems utilize the DQI in changing both the magnitude and sign of the Seebeck coefficient. For example, in the case of half-stacked of FC2 molecule, the coupling between two molecules results in the appearance of destructive interference features, which results in lower transmission. The decreasing of the conductance may suggest an increase in the thermopower(S). However, other configurations for the folded carbazoles have higher transmission and the interference effects disappear.

Further research could help to study phonon properties through the Folded carbazoles' molecular junctions and explore the thermal phonon conductance[6]. Furthermore, Quantum interference can also be controlled by charge transfer complexes [7]. This stacking framework can be expanded by investigating the electronic and phonon properties (i.e. designing materials with high thermal efficiency) of the folded carbazoles molecules with adding electron donor or acceptor such as TCNE or TTF. It would be interesting to examine how the electrical conductance will differ in the folded carbazoles with a ridged tether, controlling the space between the molecules thus allowing an acceptor or donor to bind between them. Also, many other aspects in this project deserve further attention, including Fano resonances and the examined effect of different connectivity (e.g. para and meta) in the presence of electron donor or acceptor, which may be a useful method of controlling electrical conductance and thermoelectricity. This project provides a great experimental and theoretical platform to design various molecules with specific separations, allowing other types of molecules to be part of the stacked system devices.

Bibliography

[1] Bailey, S., Visontai, D., Lambert, C. J., Bryce, M. R., Frampton, H., and Chappell, D. (2014). A study of planar anchor groups for graphene-based single-molecule electronics. *The Journal of chemical physics*, *140*(5), 054708.

[2] Hui, V. C. and Lambert, C. J. (1993). Andreev scattering, universal conductance fluctuations and phase periodic transport. *EPL (Europhysics Letters)*, *23*(3), 203.

[3] Lambert, C. J., Raimondi, R., Sweeney, V. and Volkov, A. F. (1997). Boundary conditions for quasiclassical equations in the theory of superconductivity. *Physical Review B*, *55*(9), 6015.

[4] Nolas, G. S., Sharp, J. and Goldsmid, J. (2013). *Thermoelectrics: basic principles and new materials developments* (Vol. 45). Springer Science & Business Media.

[5] Al-Khaykanee, M. K., Ismael, A. K., Grace, I. and Lambert, C. J. (2018). Oscillating Seebeck coefficients in π-stacked molecular junctions. *RSC advances*, *8*(44), 24711-24715.

[6] Kambili, A., Fagas, G., Fal'ko, V. I., & Lambert, C. J. (1999). Phonon-mediated thermal conductance of mesoscopic wires with rough edges. Physical review b, 60(23), 15593.

[7] E. Article *et al.*, "Chemical Science Charge transfer complexation boosts molecular conductance through Fermi level pinning †," pp. 2396–2403, 2019.